Supporting Information for

Mechanistic Insight into Hydrogen-Bond-Controlled Crystallinity and Adsorption Property of Covalent Organic Frameworks from Flexible Building Blocks

Xinghua Guo,[a,§] Yin Tian,[b,§] Meicheng Zhang,[a] Yang Li,[a] Rui Wen,[a] Xing Li,[a] Xiaofeng Li,[a] Ying Xue,[a] Lijian Ma,*[a] Chuanqin Xia,*[a] and Shoujian Li[a]

[a] College of Chemistry, Sichuan University, Key Laboratory of Radiation Physics & Technology, Ministry of Education, No. 29 Wangjiang Road, Chengdu, 610064, P. R. China.

[b] Southwestern Institute of Physics, Chengdu 610041, People's Republic of China.

Email: ma.lj@hotmail.com; xiachqin@163.com

Table of Content

1. Materials and general procedures S3

2. Synthesis S4

3. General procedures for volatile iodine uptake and release….....S9

4. DFT calculations for hydrogen bond.....S10

5. Figure S2. FT-IR spectra.....S13

6. Figure S3. NMR spectra and crystallographic data S17

7. Figure S4. XPS spectra.....S21

8. Figure S5. PXRD patterns S23

9. Figure S6. Structural modeling and PXRD analysis…….....S26

10. Figure S7. TEM images.....S30

11. Figure S8. N_2 adsorption.....S31

12. Figure S9. TGA curves S33

13. Figure S10. Photographs to show the color change of materials.....S34

14. Figure S11. Kinetic data of the iodine adsorption.....S35

15. Figure S12. TPT-DHBD COF on a gram scale.....S39

16. Figure S13. Reusability for iodine uptake.....S40

17. Figure S14. Photographs to show iodine enrichment in hexane.....S41

18. Figure S15. Photographs to show iodine release in ethanol.....S43

19. Table S7. Elemental analysis S44

20. Table S8. Iodine uptake data with time S44

21. Table S9. Iodine release data with time.....S45

22. Table S10. Porosity parameters and iodine uptake.....S45

23. Table S11. Comparison of iodine uptake properties of porous materials S46

1. Materials and general procedures

All the reagents and solvents are commercial available, and used without further purification. All the reactions were performed under ambient atmosphere using oven-dried glassware unless otherwise mentioned. The IR (KBr pellet) spectra were recorded (400-4000 cm^{-1} region) on Nicolet Nexus 670FT-IR and NEXUS 670 spectrometer. ^{1}H and ^{13}C NMR experiments were carried out on a Bruker AVANCE III HD spectrometer operating at resonance frequencies of 400 MHz. Solid ^{13}C NMR experiments were carried out on a Bruker Avance III 400 MHz. X-ray photoelectron spectroscopy (XPS) was recorded on a Kratos ASAM800 spectrometer. Powder X-ray diffraction data (PXRD) were collected on a Shimadzu XRD6100 diffractometer and Bruker D8 Advance diffractometer using Cu Kα radiation. Scanning electron microscopy (SEM) images were performed on a JEOL JSM-5900LV instrument. Transmission electron microscopy (TEM) images were performed on a FEI Tecnai G2 F20 S-TWIN instrument. The surface areas and pore investigated by nitrogen adsorption and desorption at 77.3 K using ASAP 2020 V4.00 from USA. The pore-size-distribution curves were obtained from the adsorption branches using non-local density functional theory (NLDFT) method. Thermogravimetric analyses (TGA) were carried out under N2 atmosphere with a heating rate of 10 ℃/min on a Shimadzu DTG-60(H) analyzer. Raman spectra were recorded on a LabRAM HR spectrometer. Element analysis (EA) were performed on a CARLO ERBA 1106.

2. Synthesis

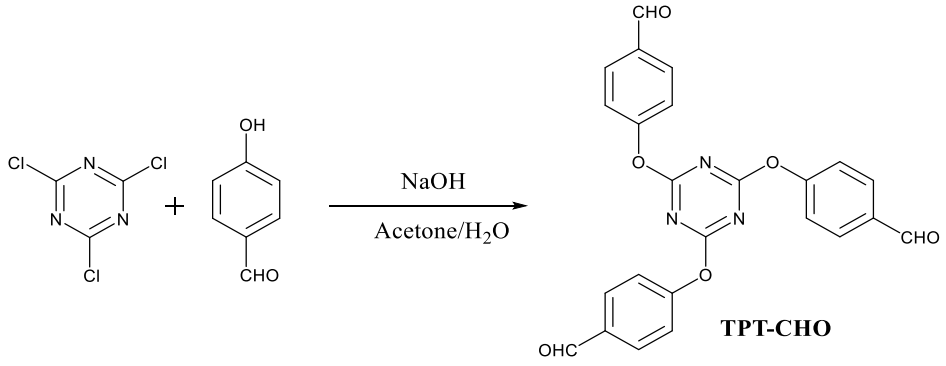

2.1 Synthesis of 2,4,6-tris-(4-formylphenoxy)-1,3,5-triazine (TPT-CHO): 4-Hydroxybenzaldehyde 7.4 g (61.0 mmol) and sodium hydroxide 2.5 g (62.0 mmol) dissolved in a mixture of acetone and water (100 mL, v/v 1:1), which was added dropwise to a stirred mixture of cyanuric chloride 3.7 g (20.0 mmol) in acetone (50 mL) at 0 ℃ for 1 h. After refluxed for 2 h, reaction mixture was poured into water (300 mL) and produced white solid product. The solid product was washed with water and 10% Na_2CO_3 and dried in vacuo. Then the powder was recrystallized from ethyl acetate to afford a white crystalline solid. Yield: (7.8 g, 88.9%).^{1}H NMR (400 MHz, $CDCl_3$) δ:9.99 (s, 3H), 7.92 (d, *J* = 8.7 Hz, 6H), 7.32 (d, *J* = 8.5 Hz, 6H).[1]

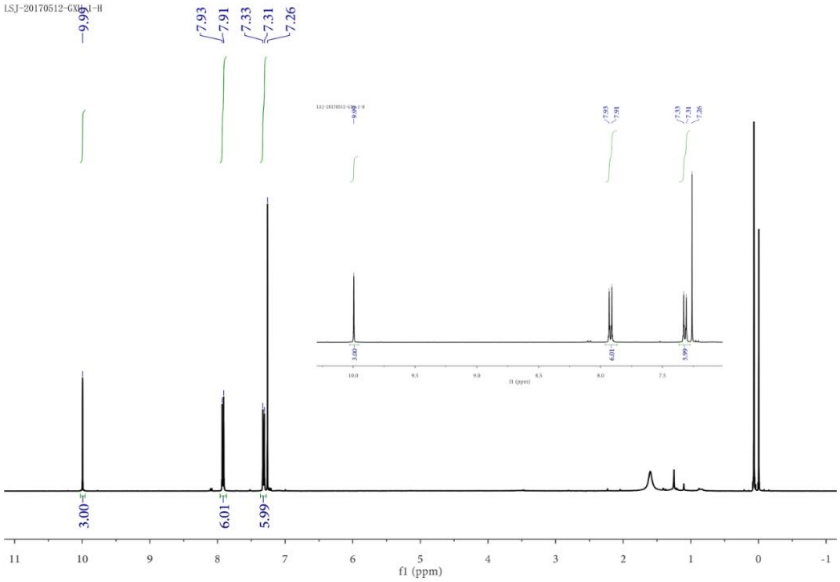

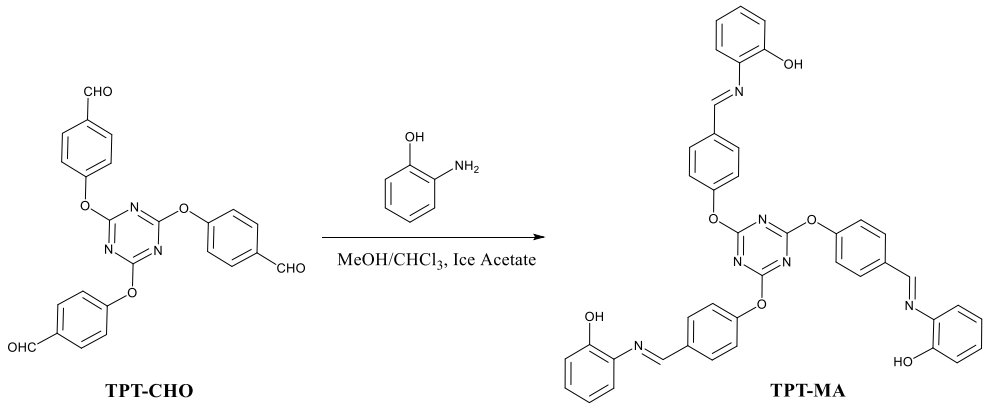

TPT-CHO **TPT-MA**

2.2 Synthesis of Model Compound A (TPT-MA): To a 50 mL flask was charged 2,4,6-tris-(4-formylphenoxy)-1,3,5-triazine (TPT-CHO, 220.0 mg, 0.5 mmol), 25 mL MeOH and 4 mL $CHCl_3$, and o-Aminophenol (220.0 mg, 2.0 mmol), then glacial acetic acid (0.2 mL) was added. The mixture was heated to reflux for 4h under inert atmosphere. After cooled to room temperature, the powder was obtained by vacuum distillation. Wash the powder with MeOH, then dried in vacuum, 241.0 mg white solid product was obtained with 68.1% yield. ^{1}H NMR (400 MHz, DMSO) δ 9.00 (s, 3H), 8.70 (s, 3H), 8.10 (d, *J* = 8.6 Hz, 6H), 7.41 (d, *J* = 8.6 Hz, 6H), 7.16 (d, *J* = 6.9 Hz, 3H), 7.08 (s, 3H), 6.89 (d, *J* = 7.5 Hz, 3H), 6.79 (s, 3H). ^{13}C NMR (101 MHz, DMSO) δ 173.48, 158.43, 153.88, 151.74, 138.08, 134.79, 130.67, 127.99, 122.28, 119.93, 119.42, 116.49.

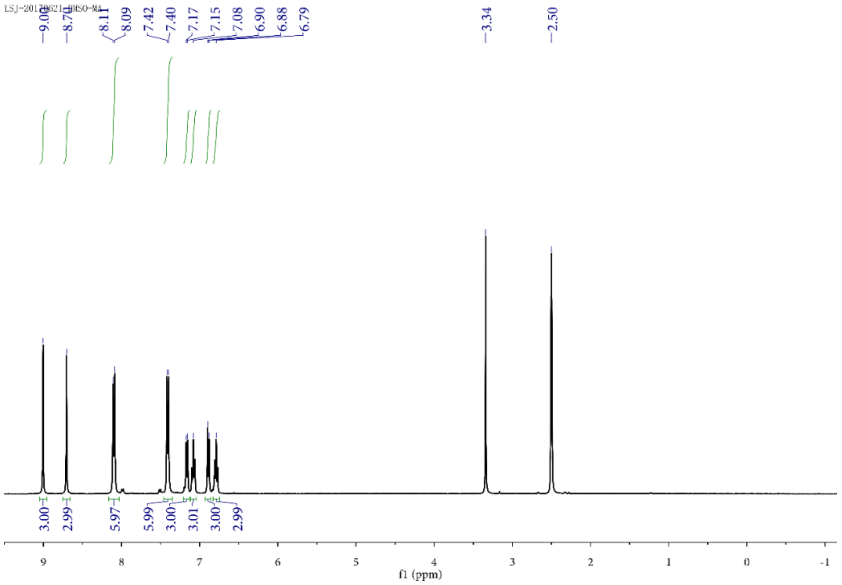

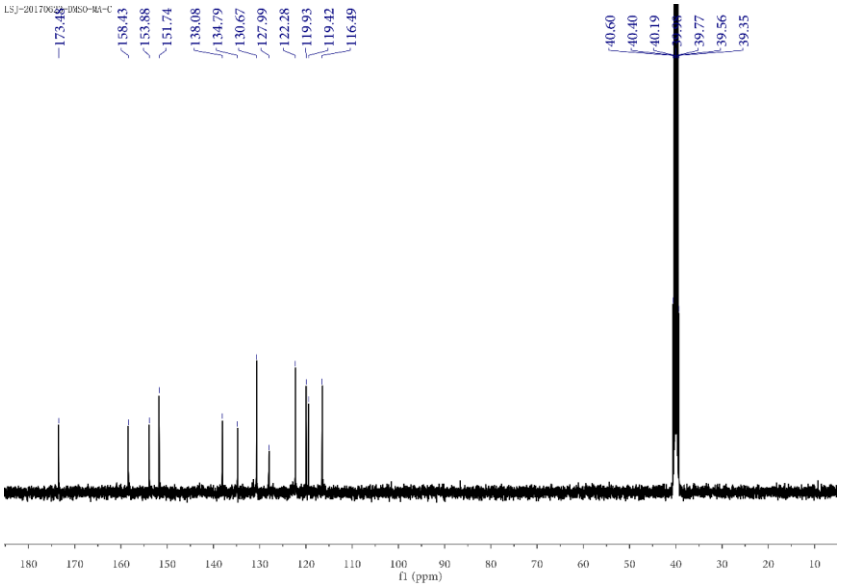

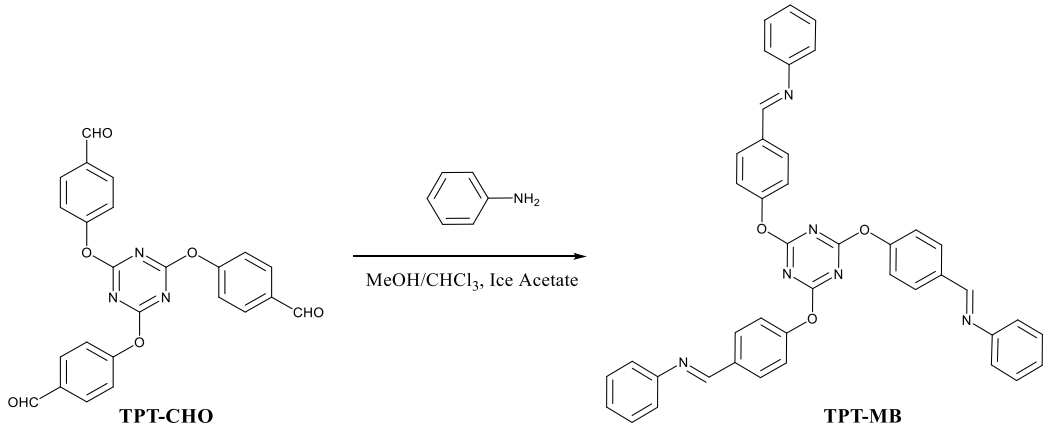

2.3 Synthesis of Model Compound B (TPT-MB): To a 50 mL flask was charged aniline (0.27 mL, 3 mmol), 25 mL MeOH, and glacial acetic acid (0.2 mL). then 2,4,6-tris-(4-formylphenoxy)-1,3,5-triazine (TPT-CHO, 220.0 mg, 0.5 mmol) was added slowly. The mixture was heated to reflux for 4h under inert atmosphere. After cooled to room temperature, the powder was obtained by vacuum distillation. Wash the powder with MeOH, then dried in vacuum, 236.0 mg white solid product was obtained with 71.0% yield. ^{1}H NMR (400 MHz, DMSO) δ 8.61 (s, 3H), 7.99 (d, J = 8.7 Hz, 6H), 7.40 (s, 12H), 7.23 (s, 9H). ^{13}C NMR (101 MHz, DMSO) δ 173.42, 160.05, 154.01, 151.77, 134.42, 130.43, 129.66, 126.51, 122.48, 121.45.

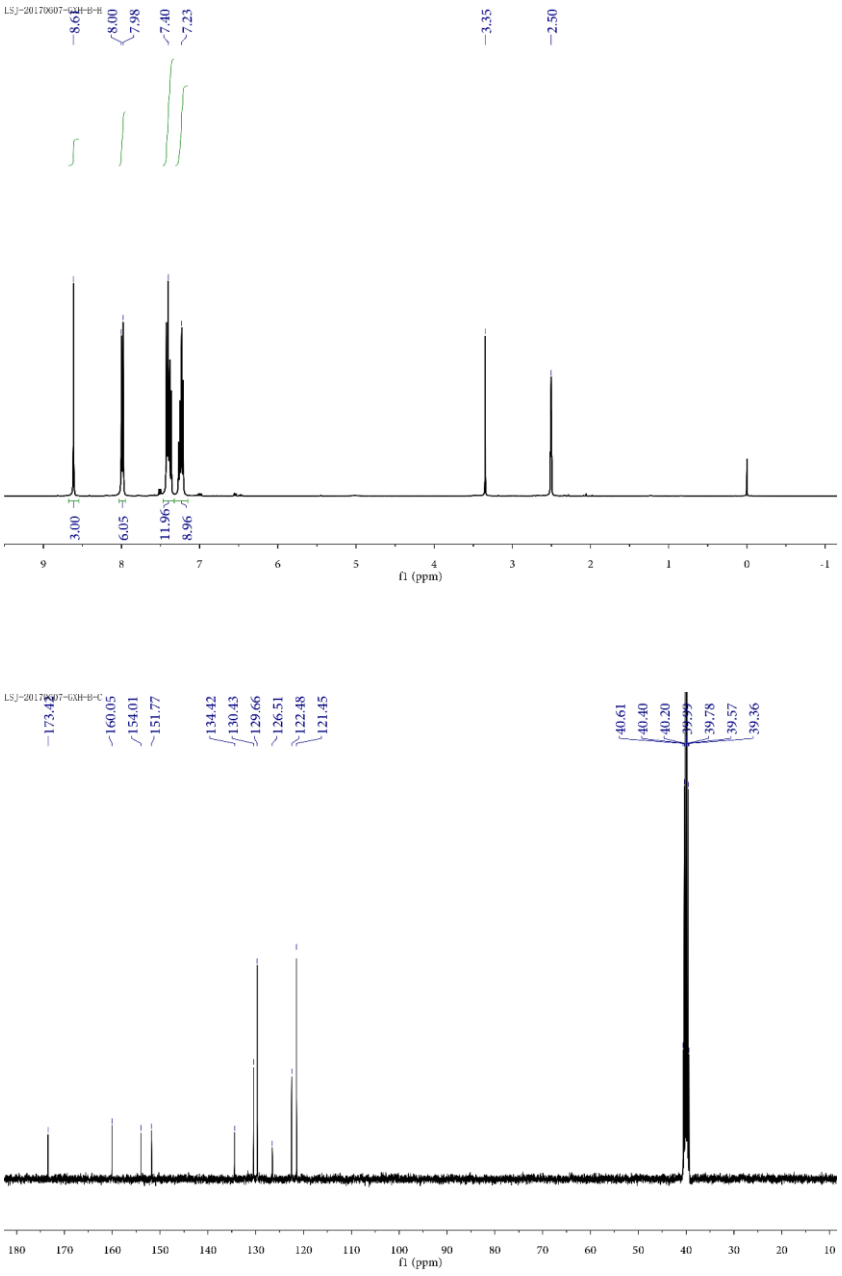

2.4 Synthesis of TPT-DHBD COF: TPT-CHO (88.4 mg, 0.2 mmol) and 3,3'-dihydroxybenzidine (DHBD) (64.8 mg, 0.3 mmol) were placed respectively in 10 mL glass vials, then mesitylene/dioxane (1:1 v/v, 1 mL) was added and the two mixtures were sonicated for 5 min to afford homogeneous dispersions. Afterwards, the two dispersions were mixed together, and the mixture was briefly sonicated for about 15 s. Subsequently, acetic acid (6 M, 0.2 mL) was slowly added and the vial was then sealed

and left undisturbed for 4 days at 80 °C. The formed solid was collected by filtration and washed with anhydrous DMF, anhydrous acetone and anhydrous THF separately until the filtrate was colorless. The resultant powder was dried at 50 °C under vacuum overnight to afford a yellowish crystalline solid in ~62.4% isolated yield and a molecular formula of $(C_{42}H_{27}N_6O_6)_n$ (% calc/found: C 70.87/65.49, H 3.83/4.05, N 11.81/9.87, O 13.49/20.63).

2.5 Synthesis of TPT-BD COF: TPT-CHO (88.4 mg, 0.2 mmol) and BD (55.2 mg, 0.3 mmol) were placed respectively in 10 mL glass vials, then mesitylene/dioxane (1:1 v/v, 1 mL) was added and the two mixtures were sonicated for 5 min to afford homogeneous dispersions. Afterwards, the two dispersions were mixed together, and the mixture was briefly sonicated for about 15 s. Subsequently, acetic acid (6 M, 0.2 mL) was slowly added and the vial was then sealed and left undisturbed for 4 days at 80 °C. The formed solid was collected by filtration and washed with anhydrous DMF, anhydrous acetone and anhydrous THF separately until the filtrate was colorless. The resultant powder was dried at 50 ºC under vacuum overnight to afford a yellow crystalline solid in ~61.3% isolated yield and a molecular formula of $(C_{42}H_{27}N_6O_3)_n$ (% calc/found: C 70.00/72.80, H 4.11/4.35, N 12.66/11.36, O 7.23/11.49).

2.6 Synthesis of TPT-DHBD$_X$ COFs (X= [DHBD] / ([BD] + [DHBD])×100): TPT-CHO (88.4 mg, 0.2 mmol) and (X=25 BD=41.4 mg, DHBD=16.2 mg; X=25 BD=27.6 mg, DHBD=32.4 mg; X=75 BD=13.8 mg, DHBD=48.6 mg) were placed respectively in 10 mL glass vials, then mesitylene/dioxane (1:1 v/v, 1 mL) was added and the two mixtures were sonicated for 5 min to afford homogeneous dispersions. Afterwards, the two dispersions were mixed together, and the mixture was briefly sonicated for about 15 s. Subsequently, acetic acid (6 M, 0.2 mL) was slowly added and the vial was then sealed and left undisturbed for 4 days at 80 °C. The formed solid was collected by filtration and washed with anhydrous DMF, anhydrous acetone and anhydrous THF separately until the filtrate was colorless. The resultant powder dried at 50 ºC under vacuum overnight to afford the crystalline solid TPT-DHBD$_X$ COFs and a molecular formula of $(C_{42}H_{27}N_6O_Y)_n$

(Y=3.75; 4.5; 5.25).

2.7 Synthesis of TPT-DHBD COF on a gram scale: TPT-CHO (1.4 g, 30 mmol) and DHBD (1.0 g, 45 mmol) were placed in a 100 mL glass vial, then mesitylene/dioxane (1:1 v/v, 20 mL) was added and the mixture was sonicated for 30 min to afford a homogeneous dispersion. Subsequently, acetic acid (6 M, 2.5 mL) was slowly added and the vial was then sealed and left undisturbed for 4 days at 80 °C. The formed solid was collected by filtration and washed with anhydrous DMF, anhydrous acetone and anhydrous THF separately until the filtrate was colorless. The resultant powder was dried at 50 °C under vacuum overnight to afford a yellowish crystalline solid in ~70.3% isolated yield.

3. General procedures for volatile iodine uptake and release

3.1 Iodine Capture: Iodine uptake experiments based on gravimetric measurements were performed in the following procedure. 10 mg of **TPT-DHBD$_X$ COFs** powder in an open glass Pyrex Beaker (2 mL) and 500 mg of iodine solids were place in a sealed glass vial (50 mL) and heated at 75 ℃ and 1.0 bar using an oven. After adsorption of the iodine vapor for a while (0-48 h), the adsorbed polymer powders were cooled down to room temperature and weighted. The iodine uptake capacities for **TPT-DHBD$_X$ COFs** were calculated by weight gains: $Cu = (W_2 - W_1) / W_1 \times 100$ wt%, where Cu is the iodine uptake capacity and W_1, W_2 are the mass weight of **TPT-DHBD$_X$ COFs** before and after adsorbed iodine vapor.

3.2 Iodine release: Iodine release and adsorbent recycle upon heating were conducted as follows: 30 mg of iodine-equilibrium **TPT-DHBD$_X$ COFs@I$_2$** powder was charged in an open glass Pyrex Beaker (2 mL) in an open glass vial (50 mL) and heated at 125 ℃ and 1.0 bar in an oil bath. The iodine release efficiency was calculated by weight gains: $Er = (30 - Wt) / W_X \times 100$ wt%, where Er is the iodine release efficiency and Wt is the mass weight of **TPT-DHBD$_X$ COFs@I$_2$** after heating release (0-420 min). W_X is the iodine

mass weight of 30 mg **TPT-DHBD$_X$ COFs@I$_2$**.

3.3 Kinetic models of the iodine adsorption of TPT-DHBD$_X$ COFs.

Three different kinetic models, namely pseudo-first-order, pseudo-second-order model and intraparticle diffusion model were employed to evaluate the controlling mechanism of the iodine adsorption process. The linear forms of the three models can be expressed by the following equations. (1) - (3) respectively.

$$\ln(q_e - q_t) = \ln q_e - k_1 t \quad (1)$$

$$\frac{t}{q_t} = \frac{1}{k_2 q_e^2} + \frac{1}{q_e} t \quad (2)$$

$$q_t = k_{int} t^{0.5} + C \quad (3)$$

where q_t refers to the amount of I_2 adsorbed (g g^{-1}) at any time t, k_1 (min^{-1}) and k_2 (g g^{-1} min^{-1}) are the pseudo-first-order and the pseudo-second-order rate constants, respectively. k_{int} (g g^{-1} min$^{-1/2}$) is the intraparticle diffusion rate constant, and C (g g^{-1}) is the constant proportional to the extent of boundary layer thickness.

4. DFT calculations for hydrogen bond

4.1 Computational details.

The electronic structure calculations for all species were performed with Kohn-Sham density functional theory (DFT)[2,3] in Gaussian 03 program.[4] The hybrid exchange-correlation functional B3LYP[5,6] was employed in this study. Moreover, the triple split valence basis set 6-311+G(d) was applied to describe hydrogen, carbon nitrogen and oxygen atoms. The geometry optimizations and energy calculations were carried out in the gas phase (298.15 K, 0.1 MPa). The harmonic frequencies were calculated to confirm the stationary point as true minimum with no imaginary frequency. The Mayer bond orders (MBO)[7,8,9] were analyzed at the same level of theory.

Figure S1. The influence of hydrogen bond on the structure of COFs. The relative energies were obtained by DFT calculations, and the Bond length (angstrom) and Mayer

bond orders (MBO) for H-bond are also shown in this figure.

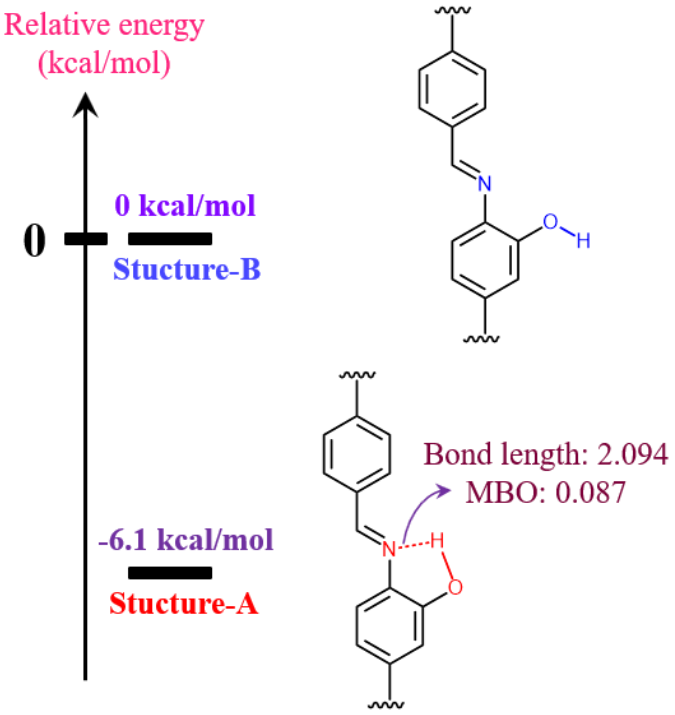

4.2 Cartesian coordinates for all optimized structures of the stationary points.

Stucture-A in Figure 4e

C	-3.91890600	0.74493300	-0.21880800
C	-2.54879400	0.95559400	-0.16873900
C	-1.67586200	-0.10974100	0.09642300
C	-2.20458300	-1.37321800	0.35124600
C	-3.57314300	-1.58388800	0.30681200
C	-4.42523100	-0.52360400	0.01406500
H	-4.56805800	1.58489100	-0.43458600
H	-1.54182600	-2.18925300	0.61672900
H	-3.97652400	-2.56764800	0.51535800
H	-5.49683500	-0.68444400	-0.01913200
C	2.47978700	0.93956900	0.40683200
C	3.83604500	1.20526400	0.45531600
C	4.75421700	0.23658500	0.05956500
C	4.30916200	-1.00051000	-0.38319000
C	2.94857900	-1.26753000	-0.43175100
C	2.02281400	-0.30135000	-0.04193600
H	1.75663700	1.68204700	0.72054000
H	4.18478100	2.16993200	0.80614900

H	5.81675700	0.44823800	0.10033600
H	5.02111800	-1.75793800	-0.69031900
H	2.59911800	-2.23514800	-0.77798000
C	0.59340800	-0.61425800	-0.11184200
H	0.34620900	-1.64130200	-0.40412300
N	-0.31540700	0.23759100	0.13323000
O	-2.05319800	2.19231800	-0.38907100
H	-1.09290200	2.14186100	-0.25696300

Stucture-B in Figure 4e

C	3.91325300	0.63855500	0.28434200
C	2.55920600	0.92869700	0.21248400
C	1.64768700	-0.06464400	-0.17180500
C	2.13568200	-1.32693700	-0.49668500
C	3.49312200	-1.61451100	-0.43447700
C	4.38230800	-0.62846800	-0.04023000
H	4.60903400	1.41273900	0.59634300
H	1.43413600	-2.07979100	-0.83853800
H	3.85039200	-2.60126000	-0.70422700
H	5.44492800	-0.83534700	0.01197600
C	-2.50658100	0.86185500	-0.59081100
C	-3.86977000	1.07009700	-0.69816100
C	-4.76365000	0.17585000	-0.11514100
C	-4.28805100	-0.92758200	0.57806200
C	-2.92021800	-1.13642500	0.68749200
C	-2.02117700	-0.24720900	0.10413800
H	-1.79507400	1.54736200	-1.03463400
H	-4.24311200	1.93334400	-1.23758100
H	-5.83156000	0.34268700	-0.20200300
H	-4.98133400	-1.62500700	1.03433300
H	-2.54533000	-1.99838700	1.23066300
C	-0.57932500	-0.49109600	0.23223500
H	-0.29033800	-1.37536100	0.81622300
N	0.29207100	0.26988300	-0.28240300
O	2.05493000	2.15054900	0.53047500
H	2.76941500	2.75635400	0.75179600

5. Figure S2. FT-IR spectra.

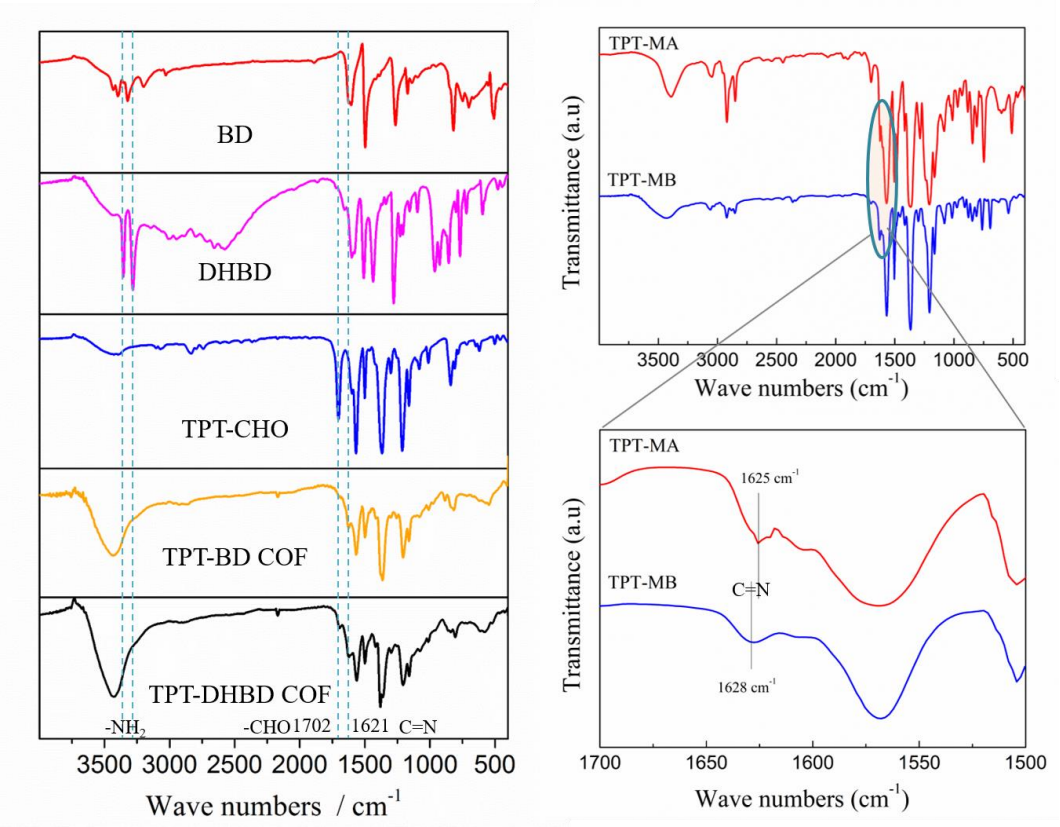

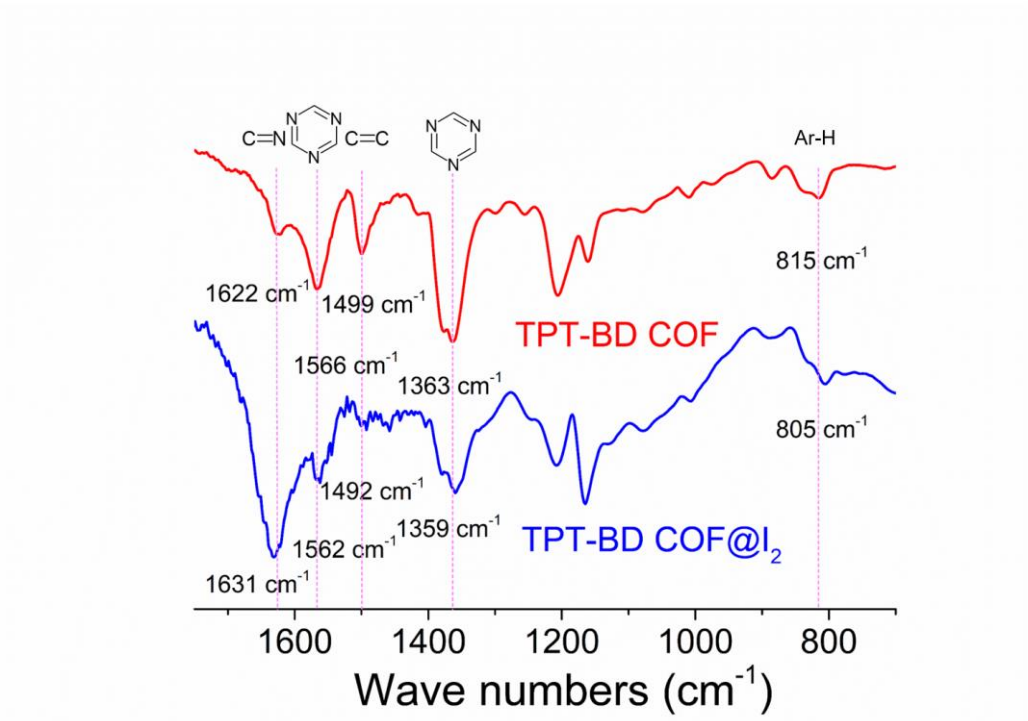

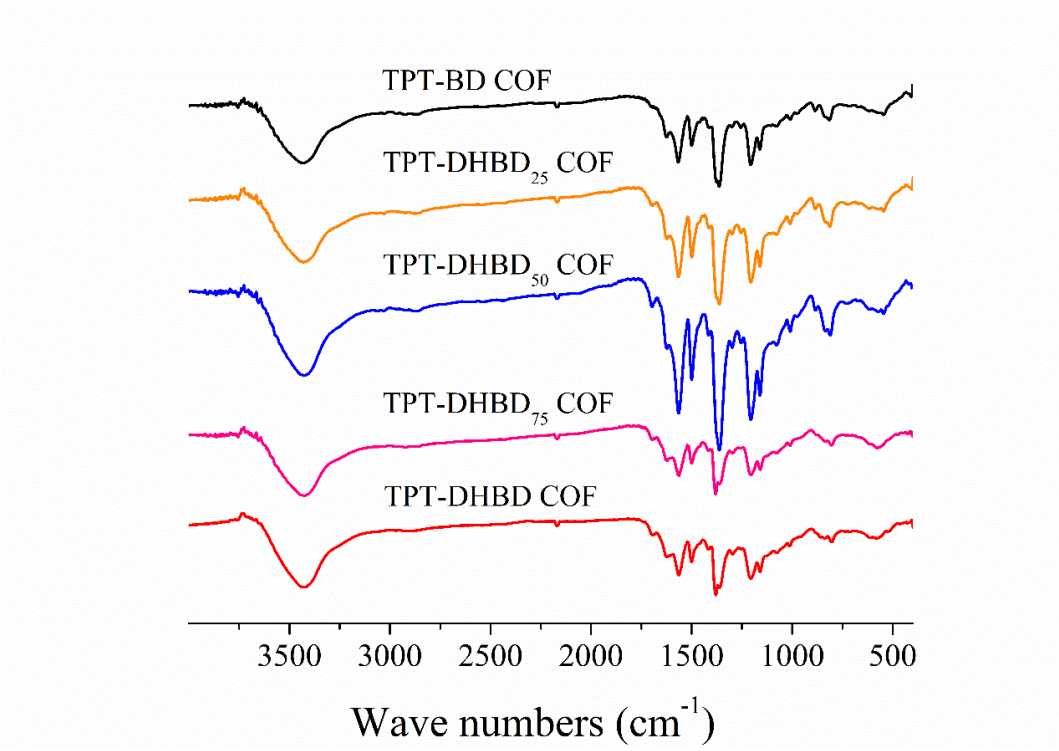
TPT-BD COF
TPT-DHBD25 COF
TPT-DHBD50 COF
TPT-DHBD75 COF
TPT-DHBD COF
3500
3000
2500
2000
1500
1000
500
Wave numbers (cm-1)

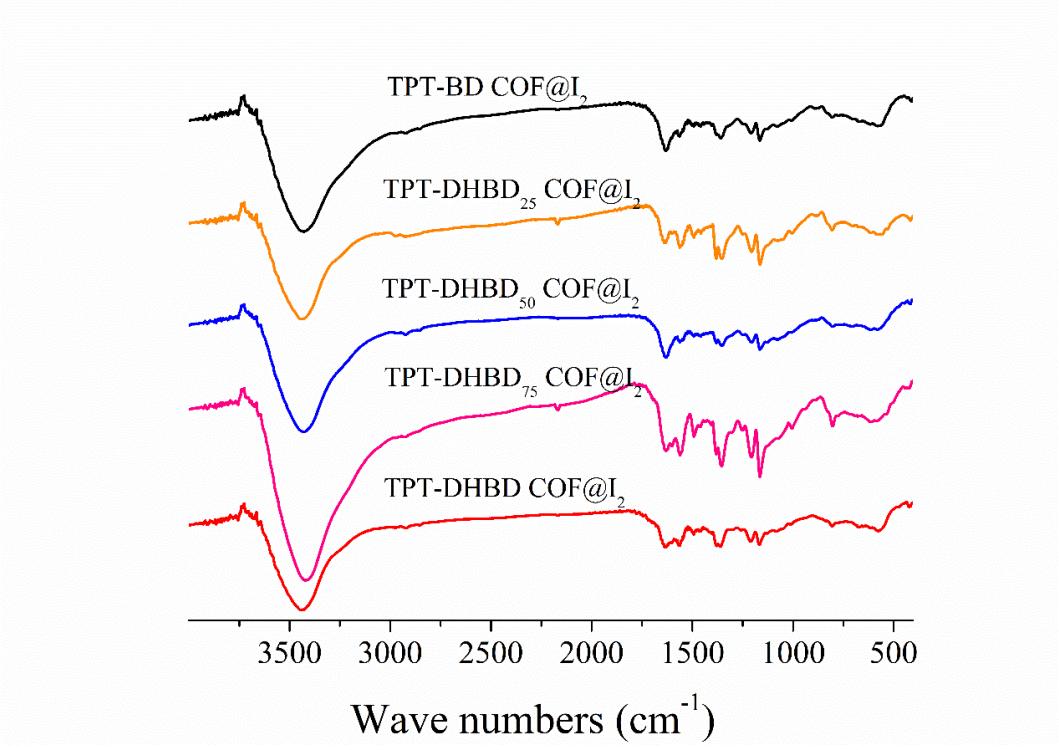
TPT-BD COF@I2
TPT-DHBD25 COF@I2
TPT-DHBD50 COF@I2
TPT-DHBD75 COF@I2
TPT-DHBD COF@I2
3500
3000
2500
2000
1500
1000
500
Wave numbers (cm-1)

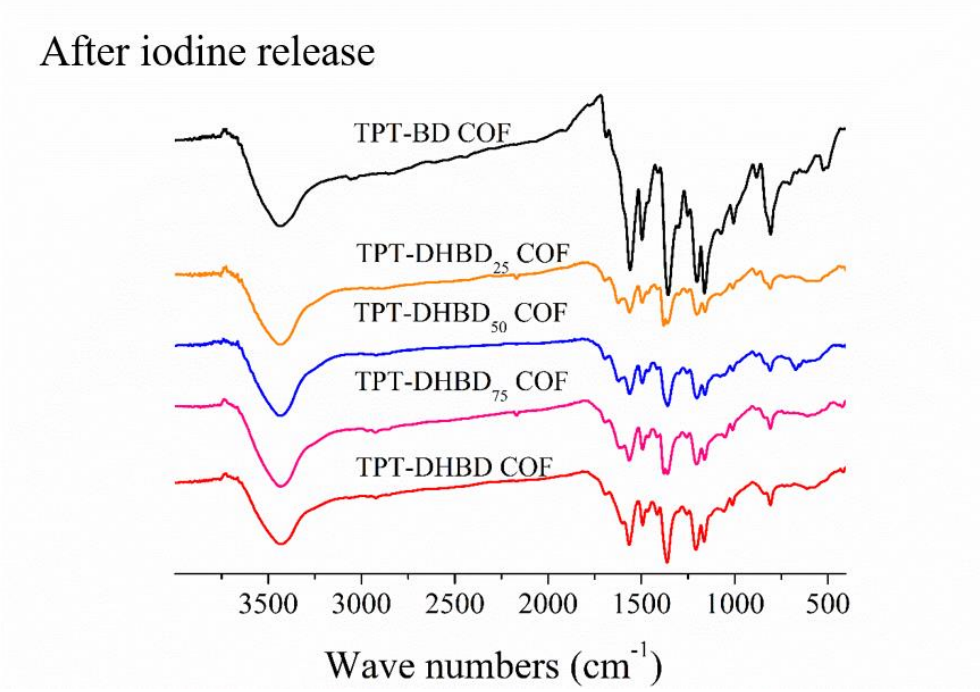

The irradiation stability of TPT-BD COF and TPT-DHBD COF after 10^5 Gy γ-ray irradiation.

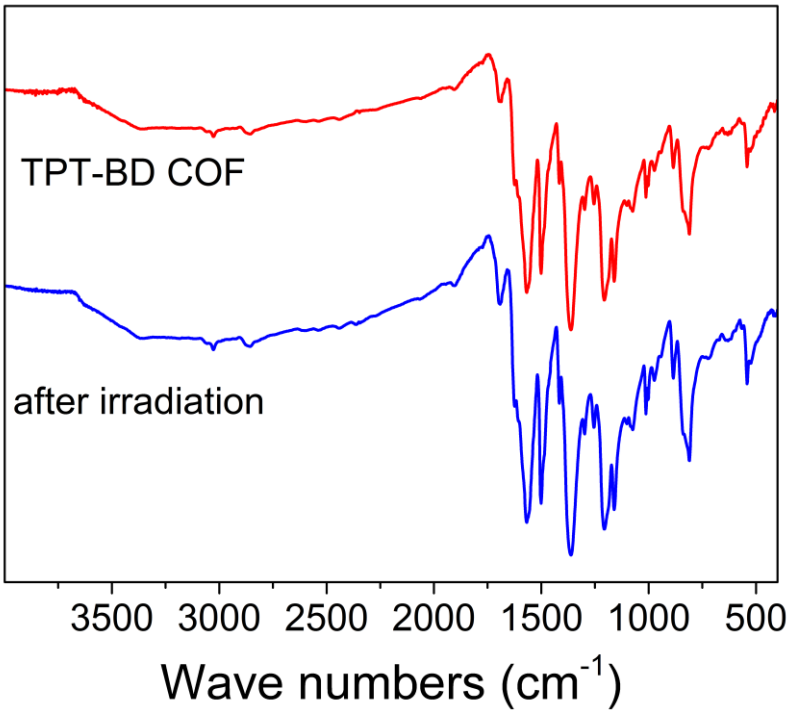

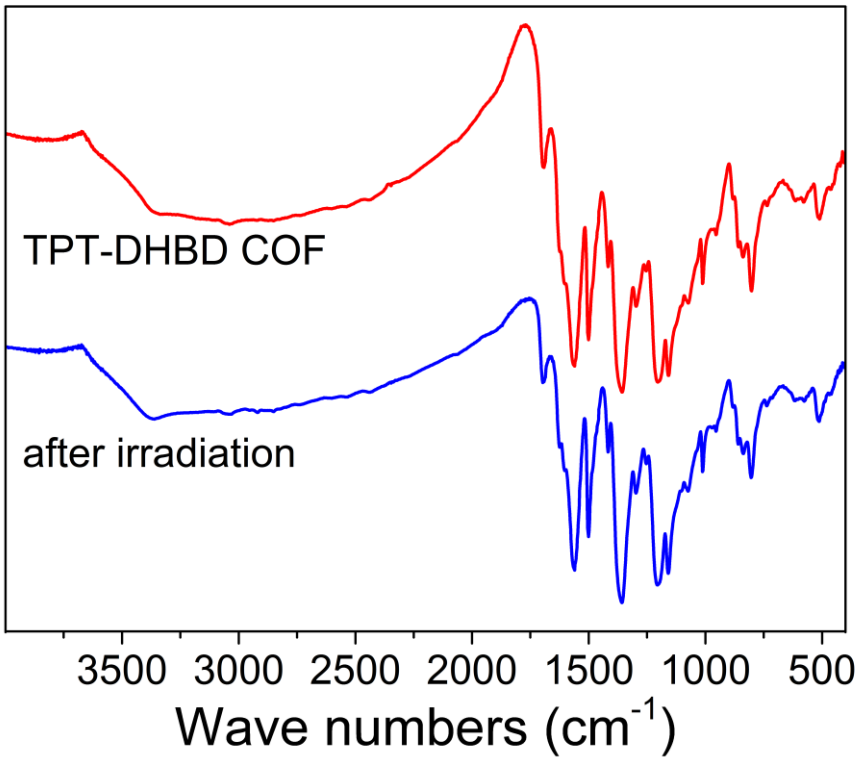

There are almost no changes in the FT-IR spectra of the materials before and after irradiation, which indicates that the as-prepared COFs possess good irradiation stabilities and can withstand 10^5 Gy γ-ray irradiation, suggesting their potentials to capture radioactive iodine, such as ^{129}I or ^{131}I in specific circumstances.

6. Figure S3. NMR spectra.

(a) The Solid-sate ^{13}C NMR spectra of TPT-BD COF.

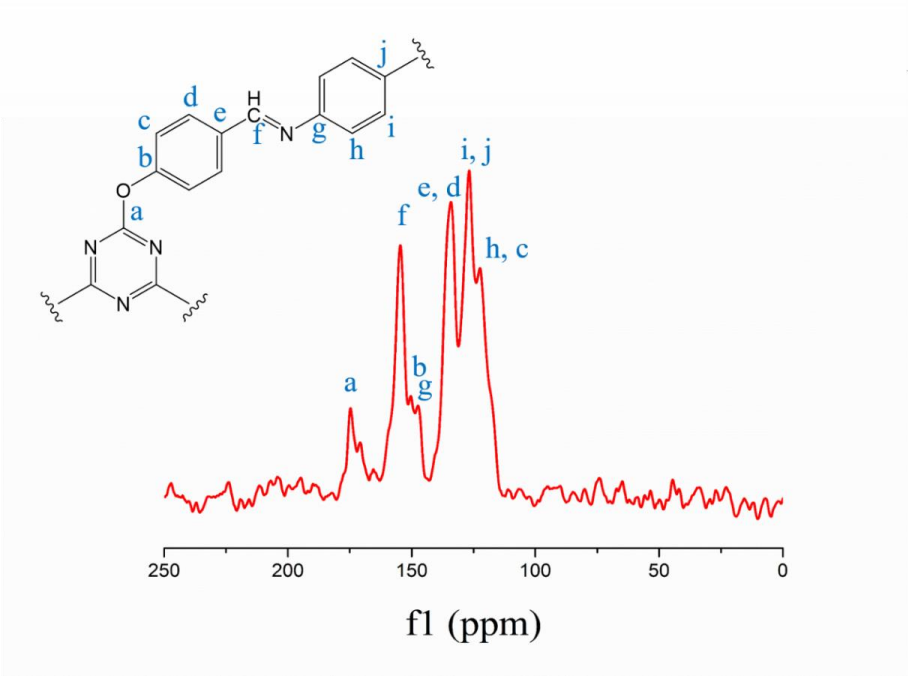

(b) The Solid-sate ^{13}C NMR spectra of TPT-DHBD COF.

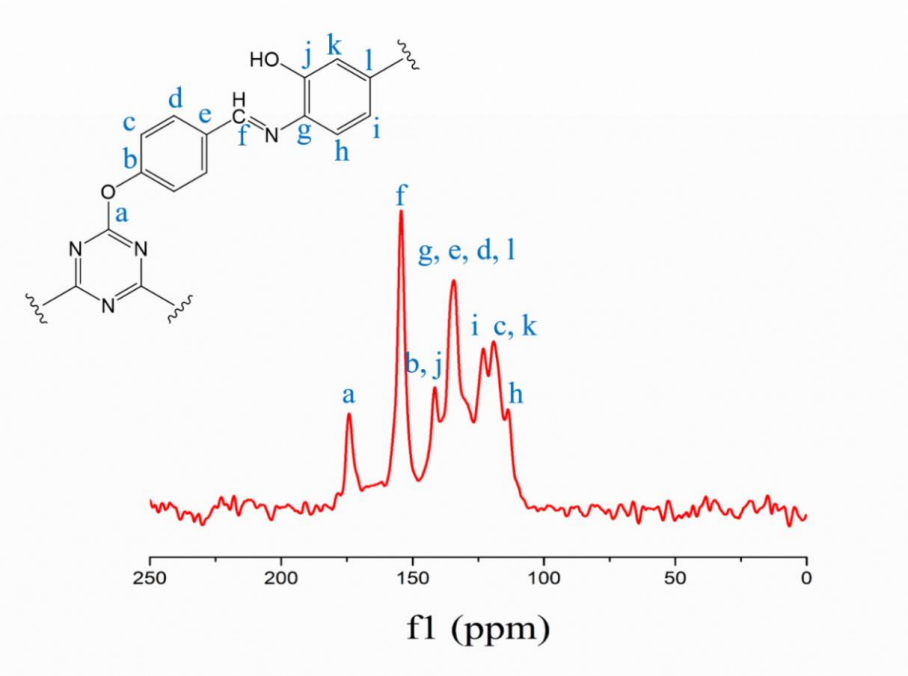

(c) ^{1}H NMR (400 MHz, $CDCl_3$) of TPT-MA.

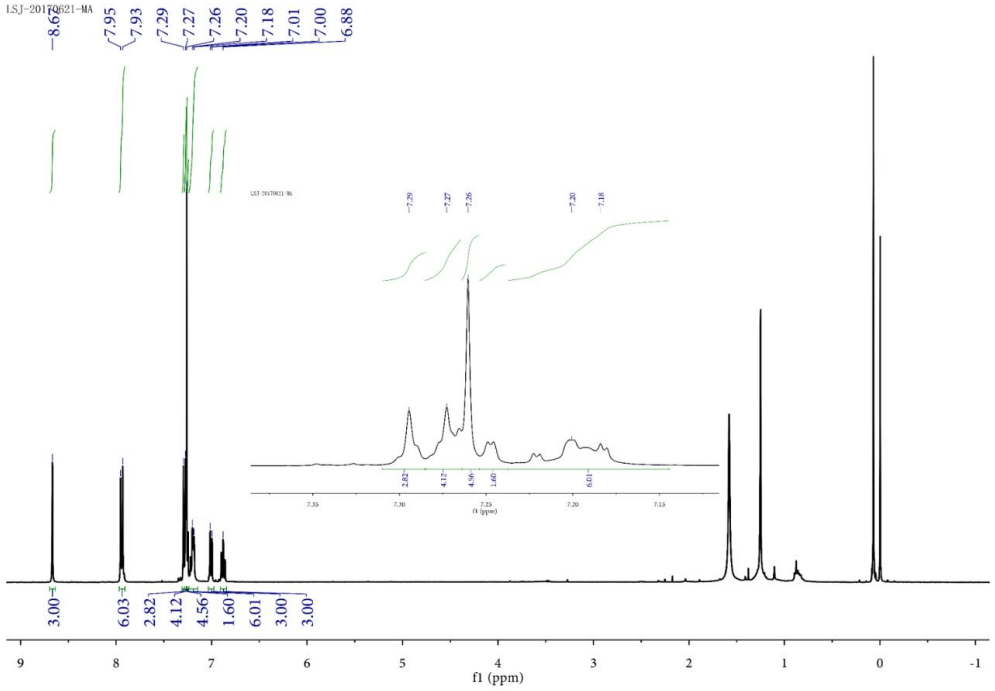

(d) ^{1}H NMR (400 MHz, $CDCl_3$) of phenol.

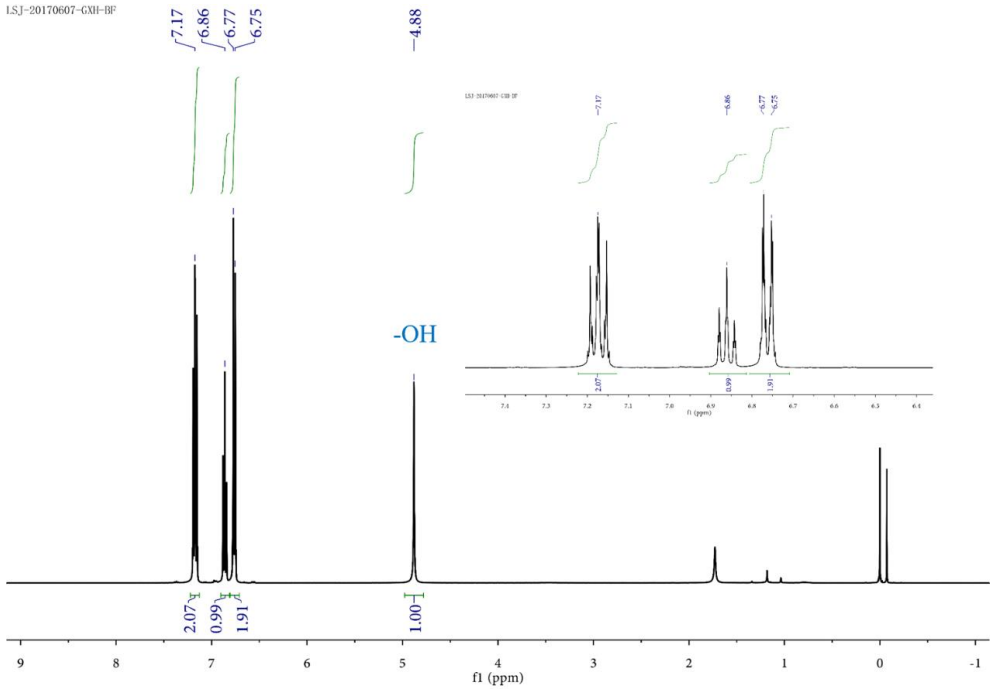

(e) ^{1}H NMR (400 MHz, DMSO) of phenol.

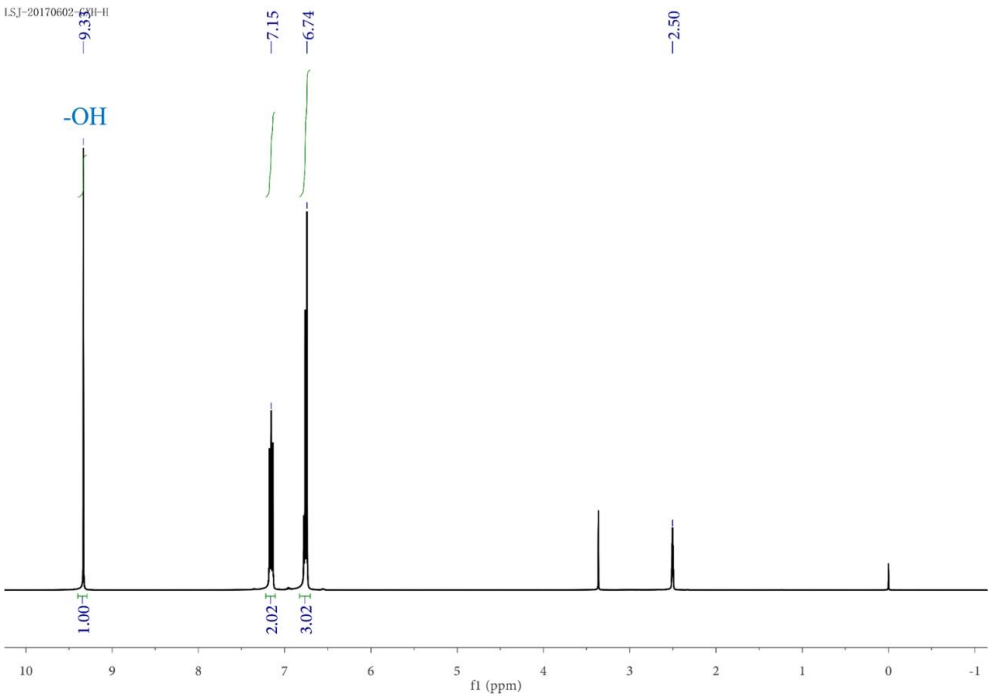

(f) ^{1}H NMR spectra of TPT-MA and TPT-MA in $CDCl_3$-d_1.

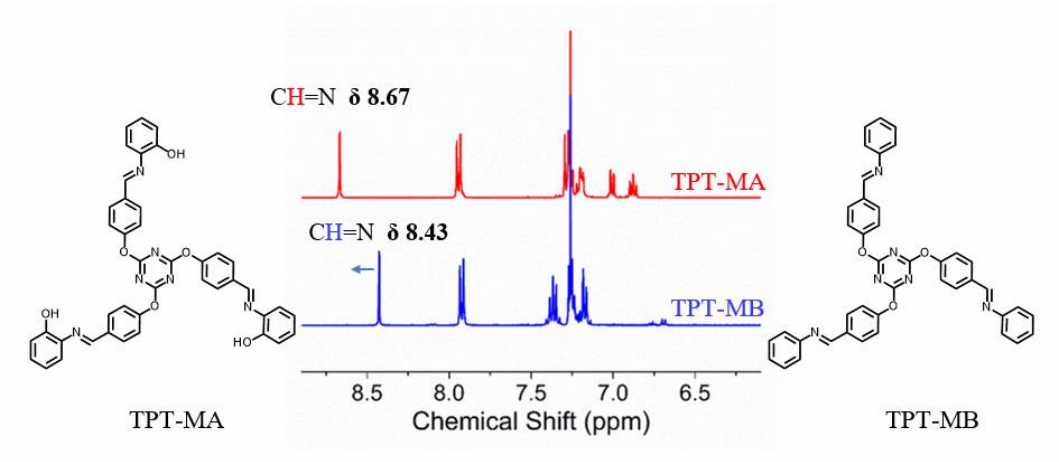

(g) The ORTEP structure and crystallographic data of compound 108 (CCDC number: 1040694).[10]

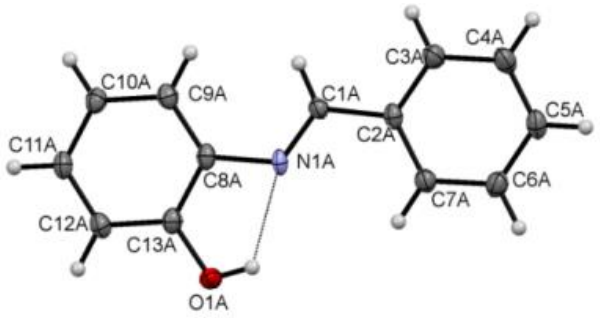

Identification code	**108**		Z′	1
Empirical formula	$C_{13}H_{11}NO$		ρ_{calc}mg/mm^3	1.299
Formula weight	197.23		μ/mm^{-1}	0.083
Temperature (K)	100		F(000)	416.0
Solvent system	ethylacetate		Crystal size/mm^3	0.2 × 0.2 × 0.1
Crystal system	orthorhombic		$\Theta_{min, max}$	5.90, 70.02°
Space group	*Pca2$_1$*		hmin, hmax; kmin,kmax ; lmin, lmax	-16 , 19; -8 , 9 ; -22 , 20
a/Å	12.1651(11)		Reflections collected	9494
b/Å	6.0020(6)		Independent reflections	4065
c/Å	13.8111(13)		R(int)	0.0185
α/°	90		Data/restraints/parameters	4065/3/148
β/°	90		Goodness-of-fit on F^2	1.052
γ/°	90		R_obs	0.0399
Volume/Å^3	1008.42(17)		wR_2(obs)	0.1059
Z	4		$\Delta\rho_{min,max}$ / e Å^{-3}	0.41/-0.19

7. Figure S4. XPS spectra.

TPT-BD COF

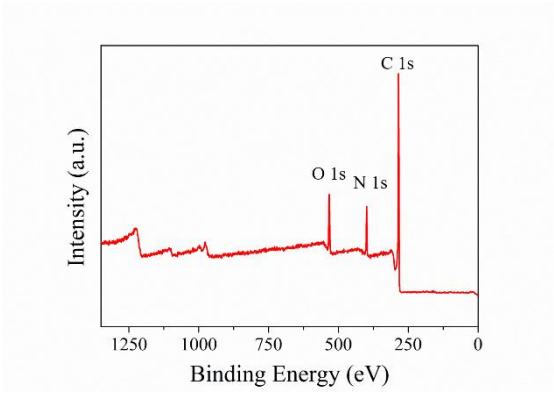

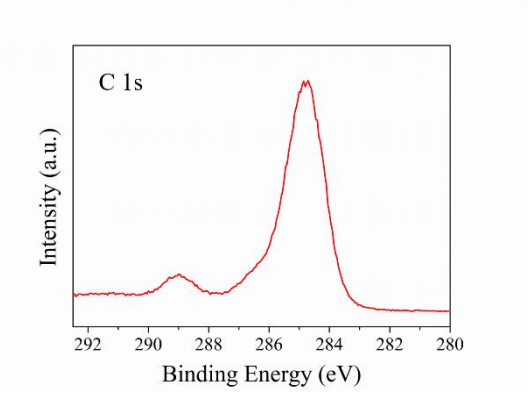

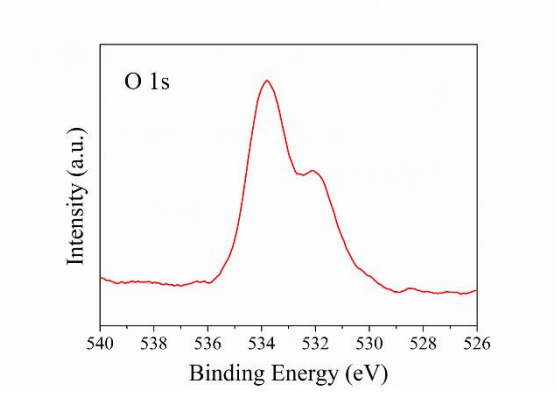

TPT-DHBD$_{50}$ COF

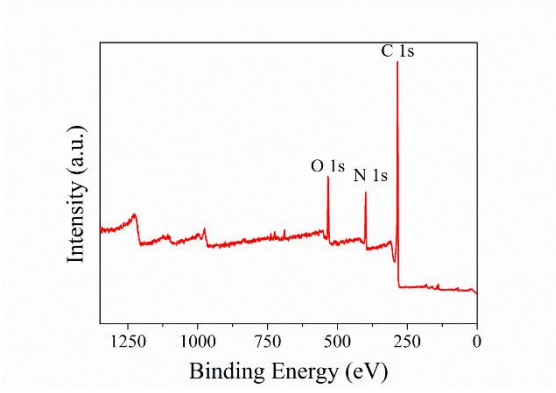

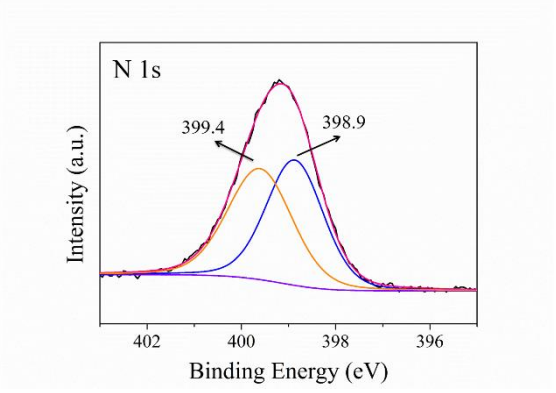

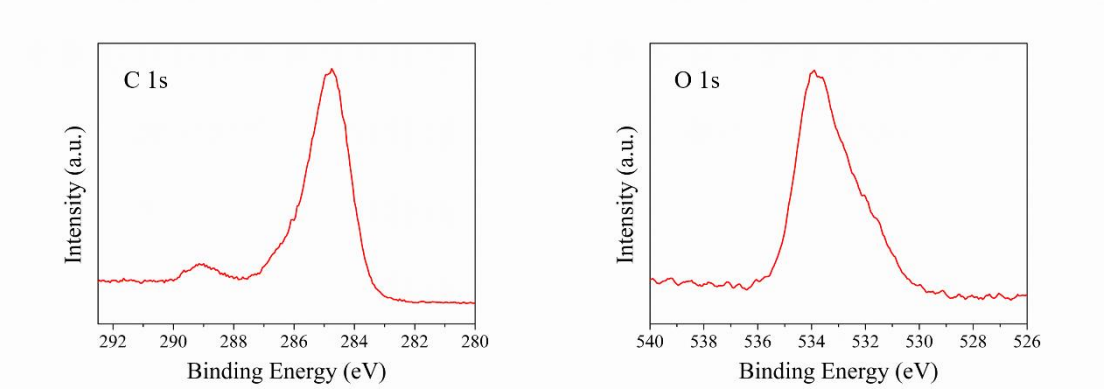
C 1s
Intensity (a.u.)
292 290 288 286 284 282 280
Binding Energy (eV)
O 1s
Intensity (a.u.)
540 538 536 534 532 530 528 526
Binding Energy (eV)

TPT-DHBD COF

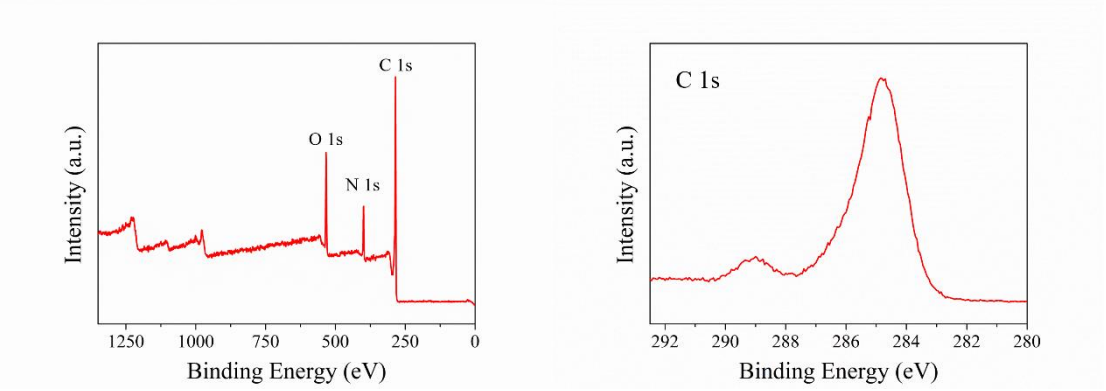
C 1s
O 1s
N 1s
Intensity (a.u.)
1250 1000 750 500 250 0
Binding Energy (eV)
C 1s
Intensity (a.u.)
292 290 288 286 284 282 280
Binding Energy (eV)

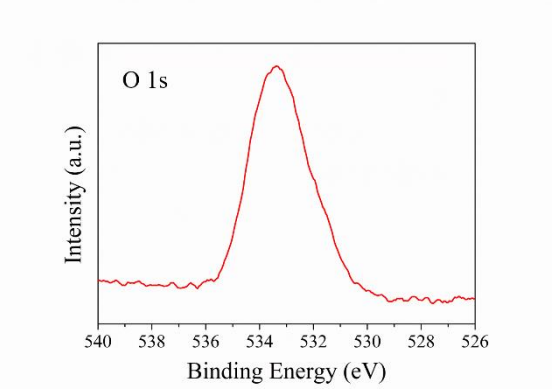
O 1s
Intensity (a.u.)
540 538 536 534 532 530 528 526
Binding Energy (eV)

8. Figure S5. PXRD patterns.

Figure S5a PXRD pattern of TPT-DHBD COF with background deduction.

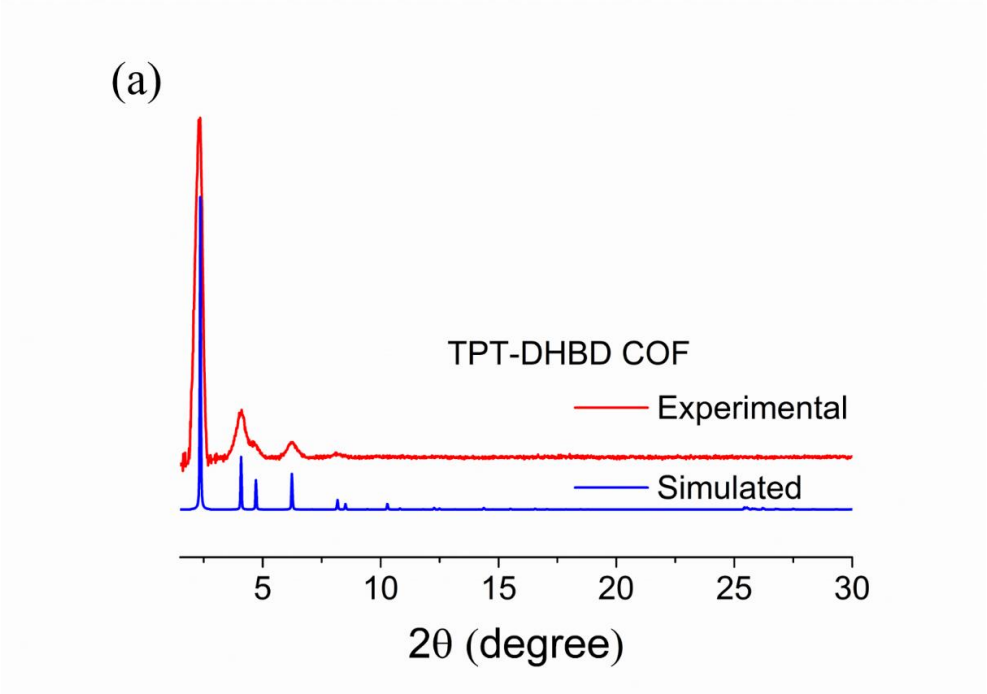

Figure S5b PXRD pattern of TPT-DHBD COF on a gram scale.

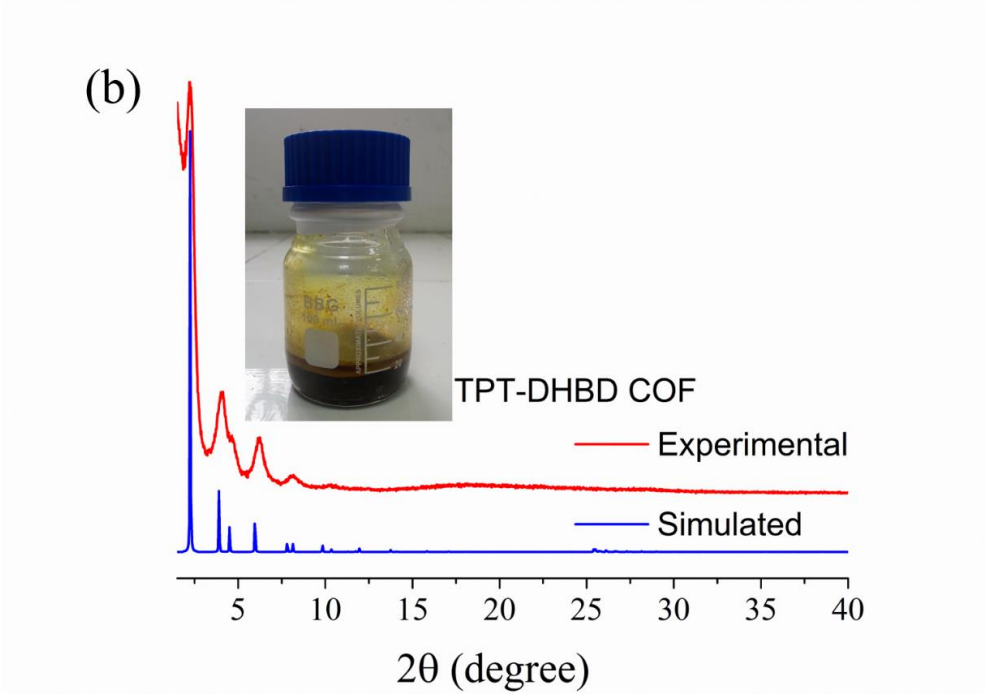

Figure S5c PXRD patterns of TPT-DHBD COF and TPT-BD COF after iodine uptake and complete release.

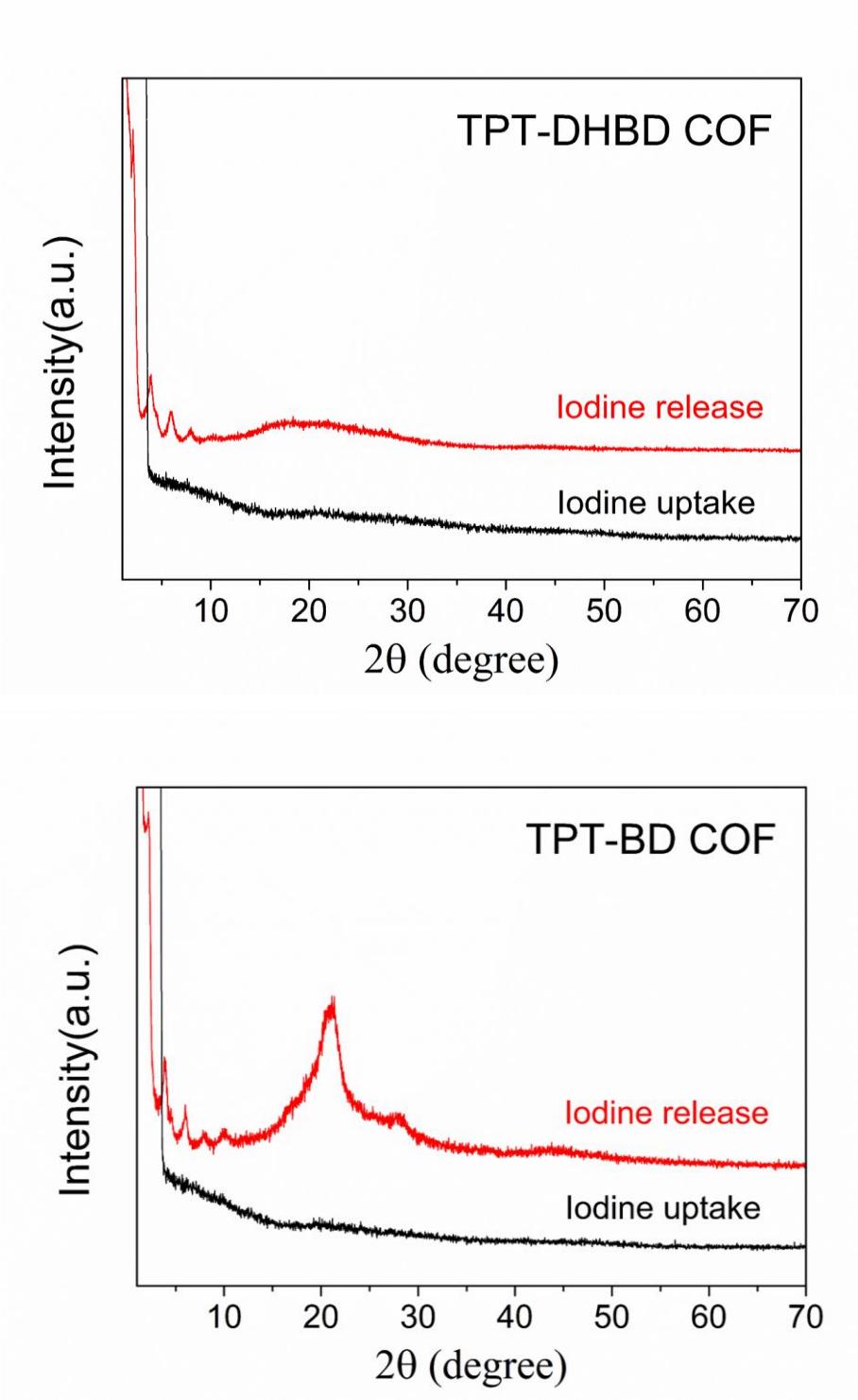

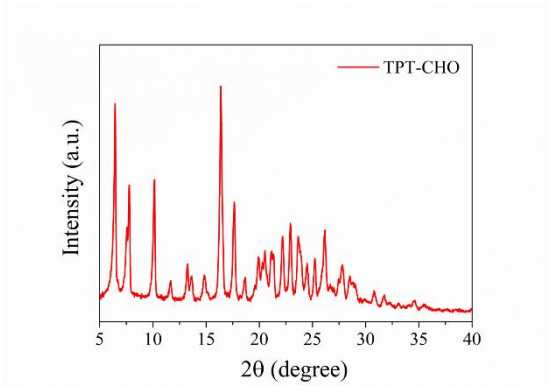
TPT-CHO
Intensity (a.u.)
2θ (degree)

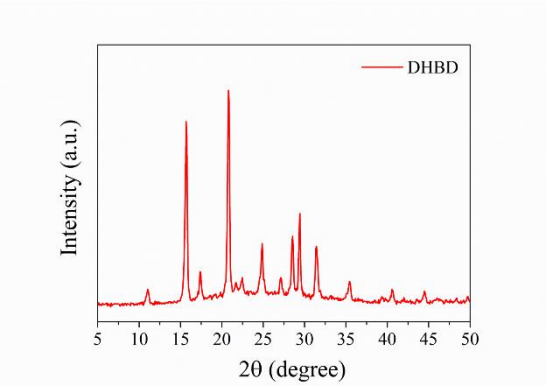
DHBD
Intensity (a.u.)
2θ (degree)

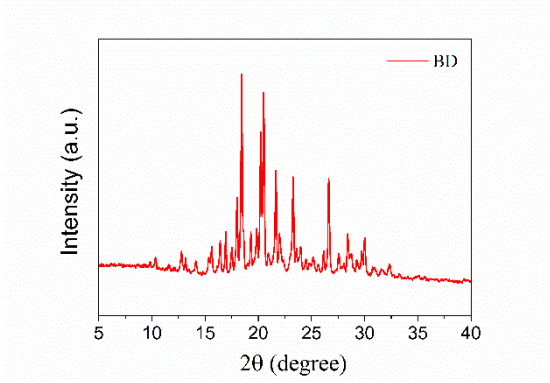
BD
Intensity (a.u.)
2θ (degree)

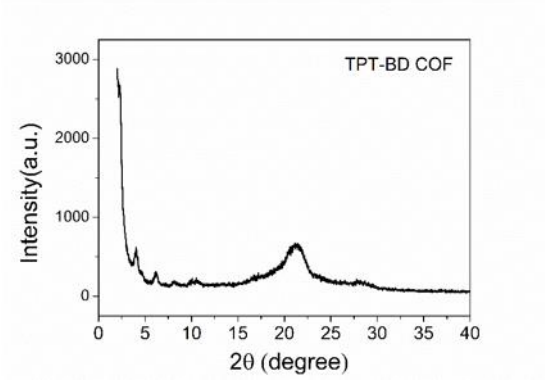
TPT-BD COF
Intensity(a.u.)
2θ (degree)

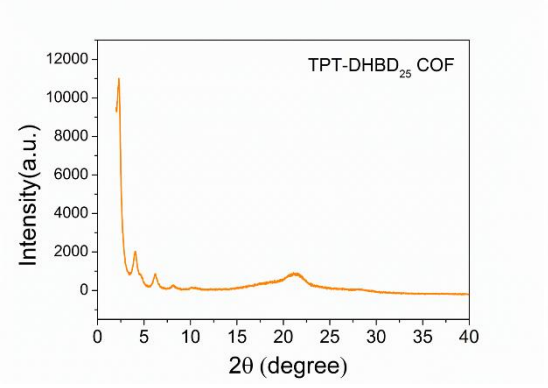
TPT-DHBD25 COF
Intensity(a.u.)
2θ (degree)

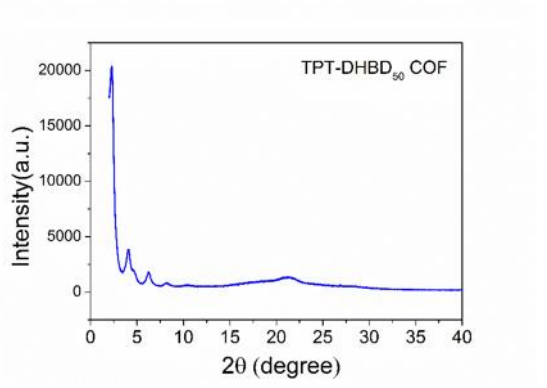
TPT-DHBD50 COF
Intensity(a.u.)
2θ (degree)

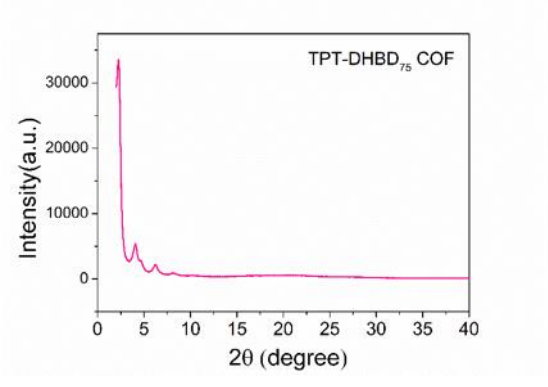
TPT-DHBD75 COF
Intensity(a.u.)
2θ (degree)

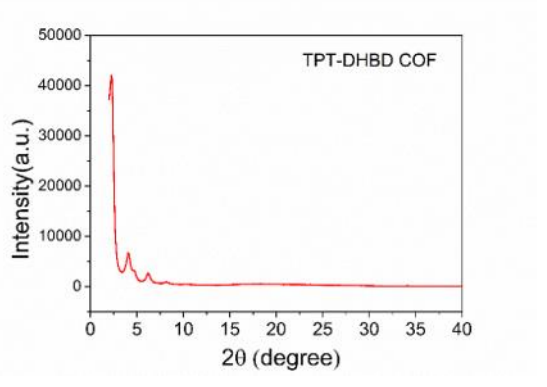
TPT-DHBD COF
Intensity(a.u.)
2θ (degree)

9. Figure S6. Structural modeling and PXRD analysis.

Figure S6a Space-filling models of TPT-BD COF with different stacking and the calculated PXRD profiles. C, gray; N, blue; O, red; H, white.

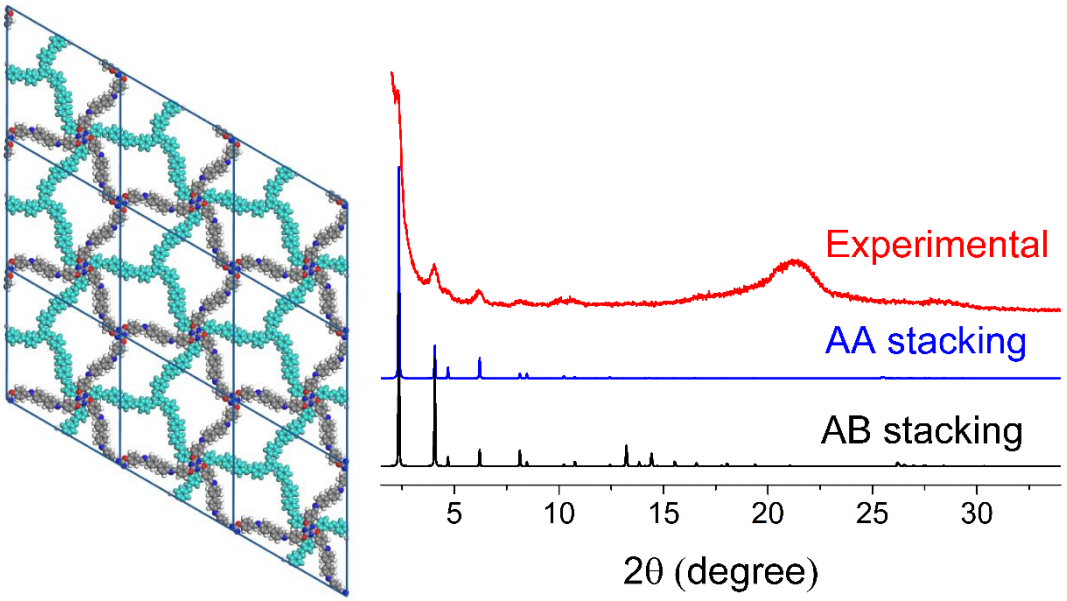

Figure S6b Space-filling models of TPT-DHBD COF with different stacking and the calculated PXRD profiles. C, gray; N, blue; O, red; H, white.

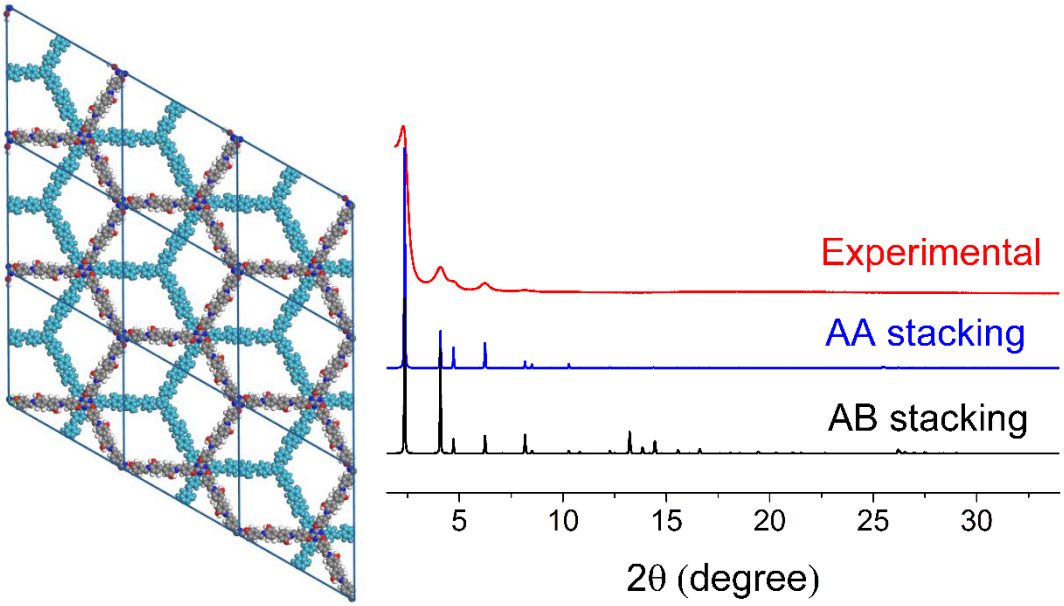

Table S1. Fractional atomic coordinates for the unit cell of TPT-BD COF.

TPT-BD COF: Space group: P6/M			
a = 43.46 Å, b = 43.46 Å, c = 3.50 Å			
α = 90°, β = 90°, γ = 120°			
Atom	x	y	z
N1	-1.35511	0.29911	0
C2	-1.32039	0.31116	0
O3	-1.40520	0.30546	0
C4	-1.32662	0.25259	0
C5	-1.36348	0.23495	0
C6	-1.38250	0.20021	0
C7	-1.36686	0.17971	0
C8	-1.33031	0.19517	0
C9	-1.31008	0.23210	0
C10	-1.39296	0.14329	0
N11	-1.38958	0.11597	0
C12	-1.08240	0.49616	0
C13	-1.07880	0.46563	0
C14	-1.04718	0.46768	0
C15	-1.01682	0.49984	0
C16	-1.01966	0.53080	0
C17	-1.05223	0.52871	0
H18	-1.38154	0.24416	0
H19	-1.41088	0.18936	0
H20	-1.31785	0.17930	0
H21	-1.28173	0.24476	0

H22	-1.41808	0.14030	0
H23	-1.09890	0.43848	0
H24	-1.04791	0.44293	0
H25	-0.99775	0.55709	0
H26	-1.05391	0.55244	0

Table S2. Fractional atomic coordinates for the unit cell of TPT-DHBD COF.

TPT-DHBD COF: Space group: P6/M			
a = 43.26 Å, b = 43.26 Å, c = 3.44 Å			
α = 90°, β = 90°, γ = 120°			
Atom	x	y	z
N1	-1.36674	0.30627	0
C2	-1.33840	0.30600	0
O3	-1.39752	0.33287	0
C4	-1.36333	0.24521	0
C5	-1.39661	0.23594	0
C6	-1.42052	0.20314	0
C7	-1.41209	0.17887	0
C8	-1.37916	0.18790	0
C9	-1.35526	0.22063	0
C10	-1.43788	0.14446	0
N11	-1.43059	0.12153	0
C12	-1.09085	0.46814	0
C13	-1.07726	0.44789	0
C14	-1.04368	0.46093	0
C15	-1.02212	0.49293	0

C16	-1.03625	0.51486	0
C17	-1.06989	0.50197	0
O18	-1.40621	0.07773	0
H19	-1.39214	0.10219	0
H20	-1.37180	0.16975	0
H21	-1.44581	0.19670	0
H22	-1.40538	0.25274	0
H23	-1.33000	0.22704	0
H24	-1.44874	0.01805	0
H25	-1.53247	0.03163	0
H26	-1.49758	0.08831	0
H27	-1.54875	0.86482	0

10. Figure S7. TEM images.

TPT-BD COF

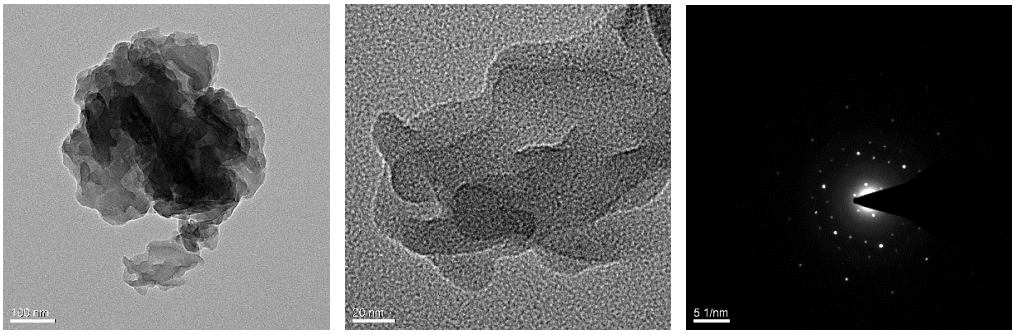

TPT-DHBD$_{50}$ COF

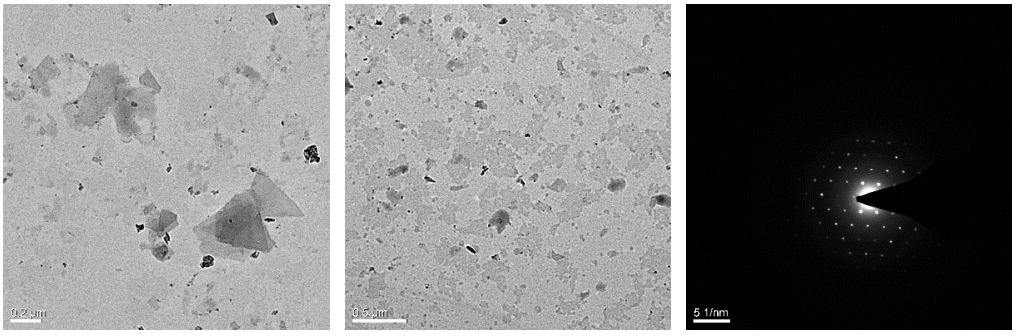

TPT-DHBD COF

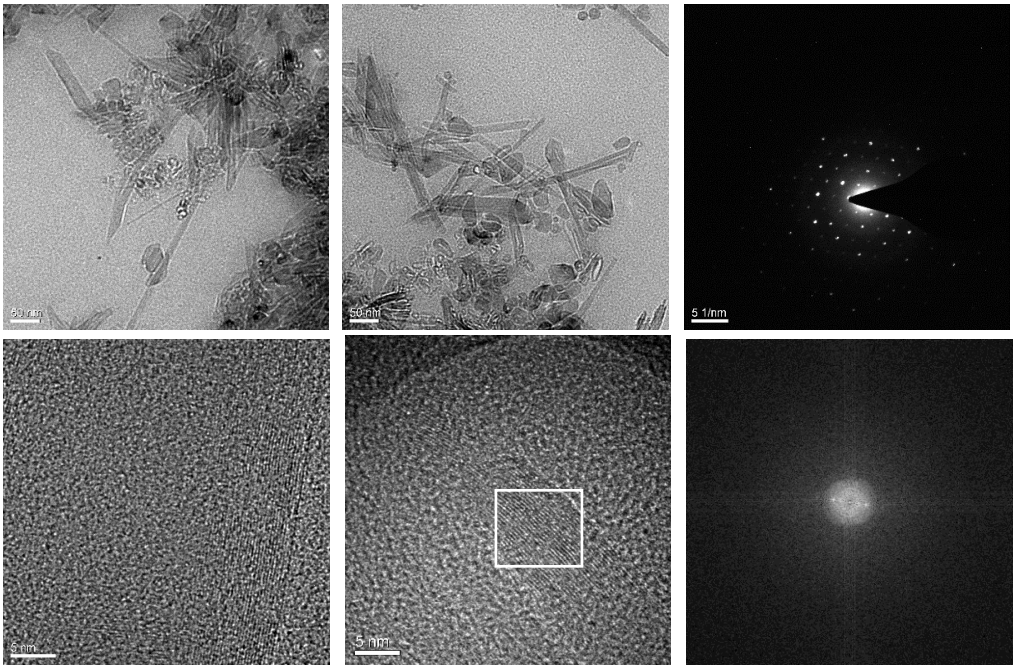

11. Figure S8. N_2 adsorption.

Figure S8a. N_2 adsorption-desorption isotherms (77 K) of TPT-DHBDx COFs.

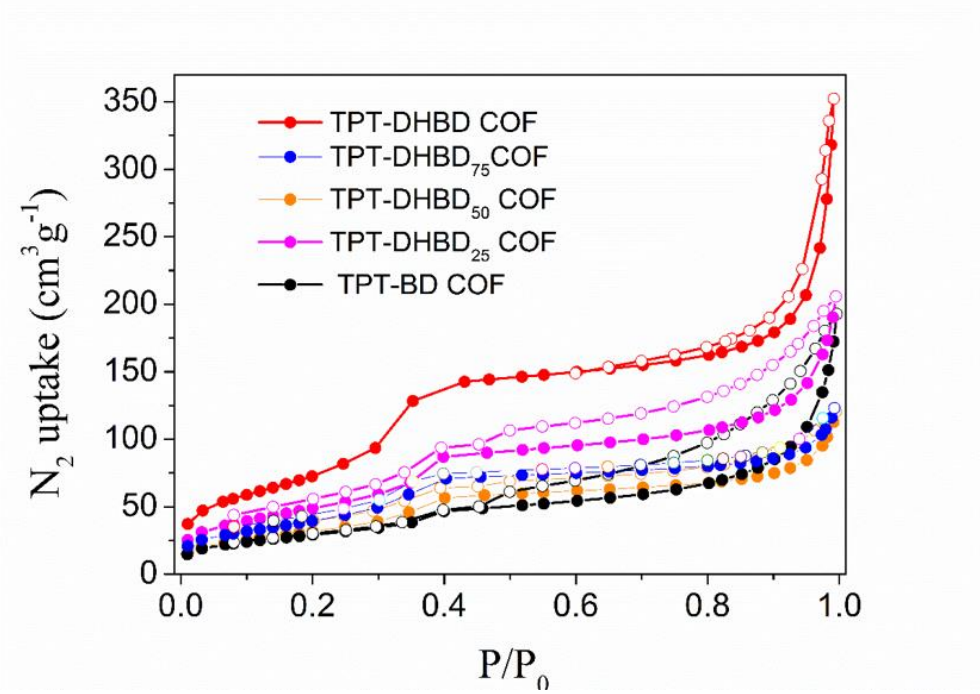

Figure S8b. Pore-size distribution of TPT-DHBDx COFs.

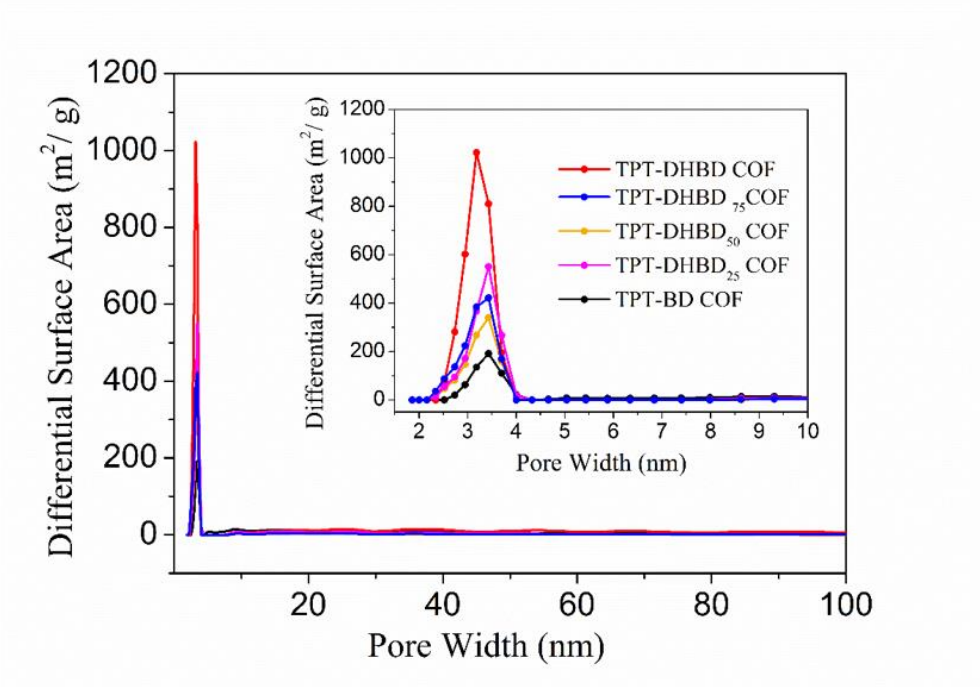

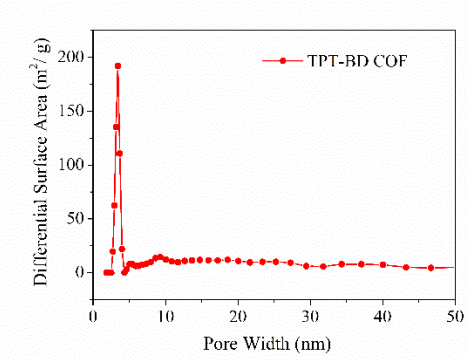
TPT-BD COF
Differential Surface Area (m²/ g)
Pore Width (nm)

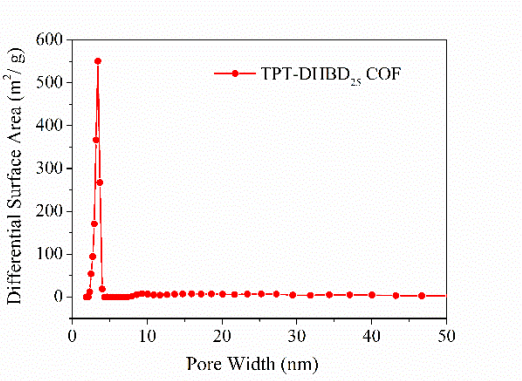
TPT-DIIBD25 COF
Differential Surface Area (m²/ g)
Pore Width (nm)

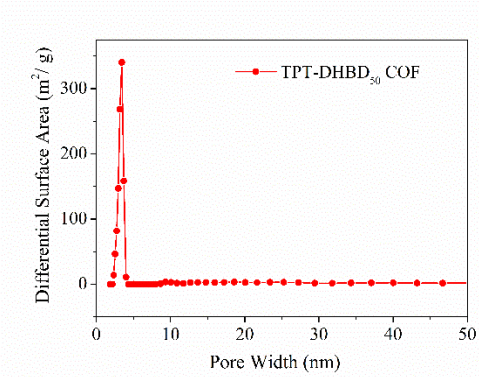
TPT-DHBD50 COF
Differential Surface Area (m²/ g)
Pore Width (nm)

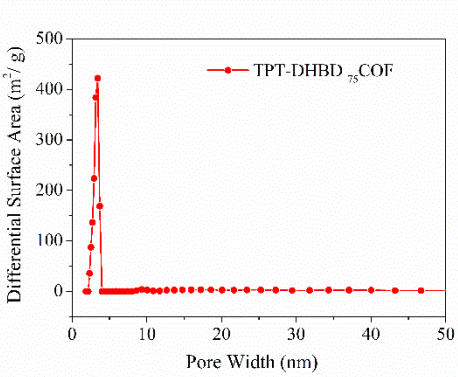
TPT-DHBD 75COF
Differential Surface Area (m²/ g)
Pore Width (nm)

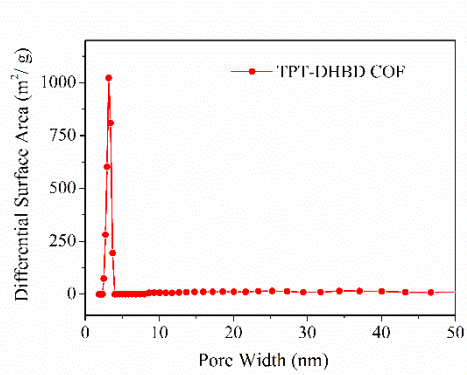
TPT-DHBD COF
Differential Surface Area (m²/ g)
Pore Width (nm)

12. Figure S9. TGA curves.

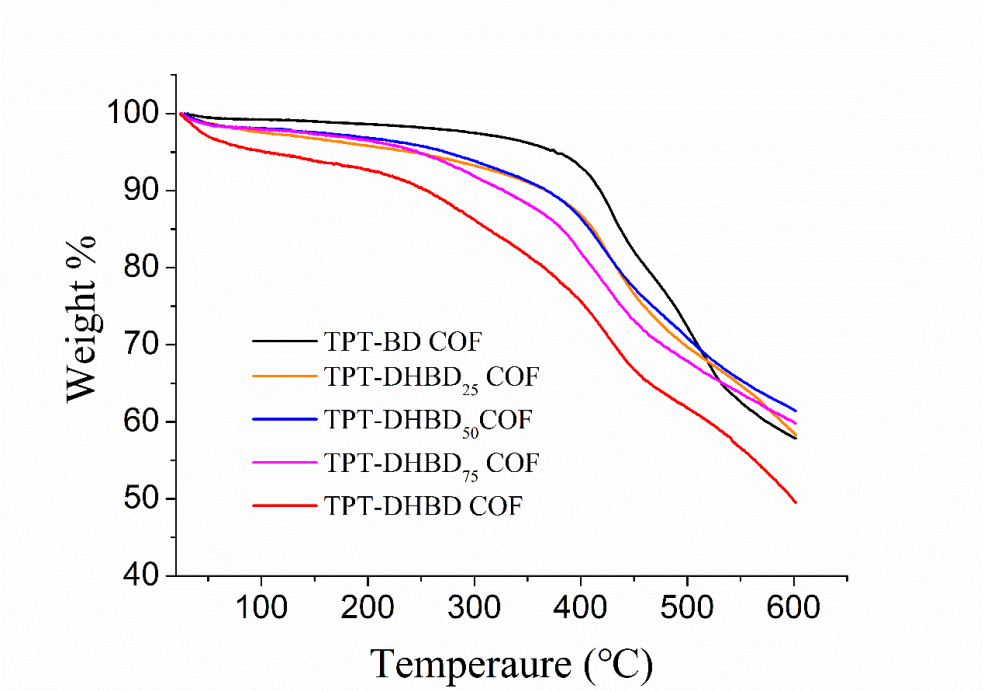

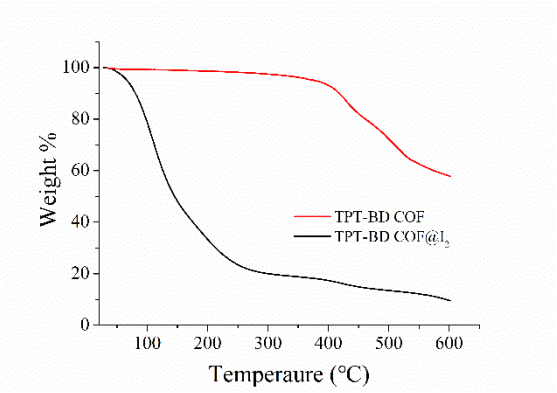

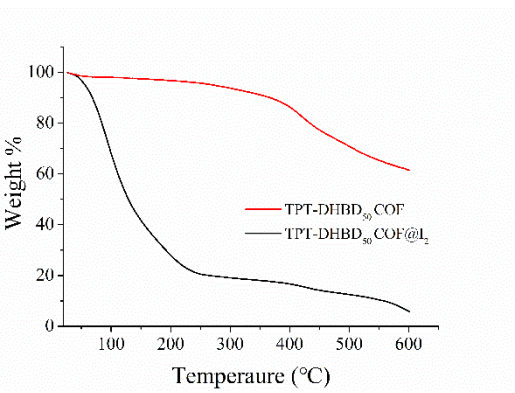

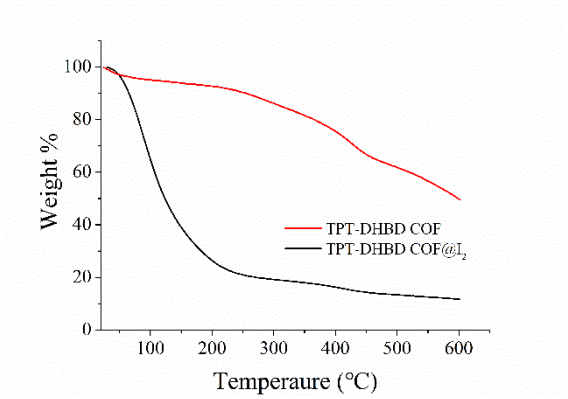

13. Figure S10. Photographs to show the color change before and after iodine uptake and release for TPT-DHBD$_X$ COF.

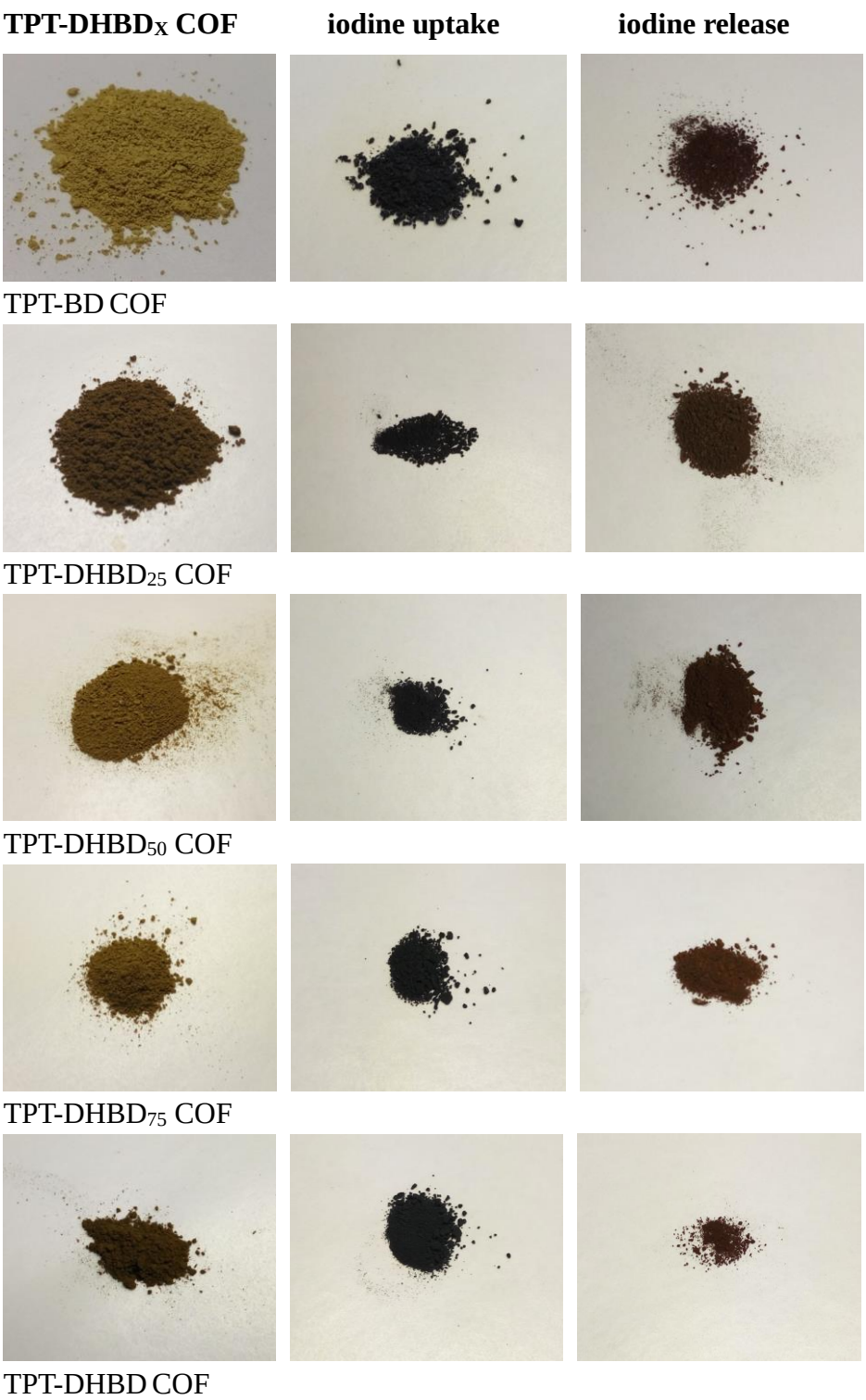

14. Figure S11. Kinetic data of the iodine adsorption of TPT-DHBD$_X$ COFs.

Fig. S11a (a) Pseudo-first-order, (b) pseudo-second-order and (c) intraparticle diffusion model plots for the iodine adsorption onto TPT-BD COF.

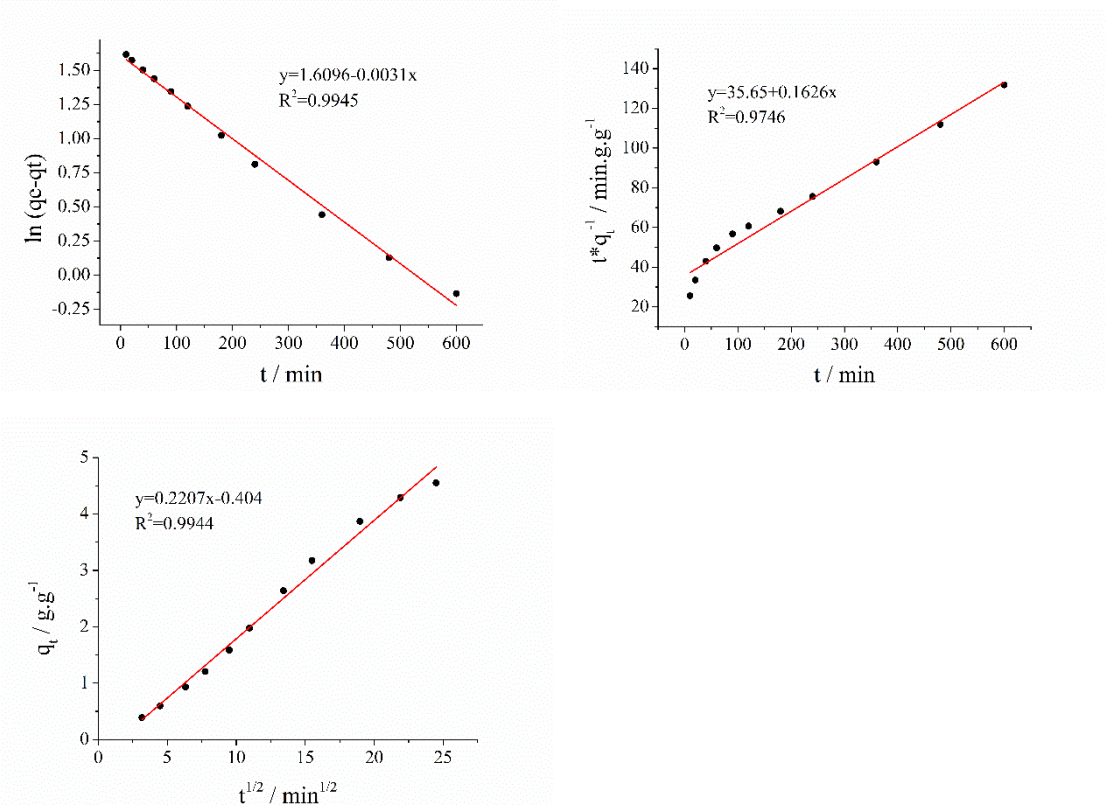

Table S3. Kinetic parameters for the iodine adsorption onto TPT-BD COF.

q_e (exp)	pseudo-first-order			pseudo-second-order		
(g g^{-1})	q_e (g g^{-1})	k_1 (min^{-1})	R^2	q_e (g g^{-1})	k_2 (g g^{-1} min^{-1})	R^2
5.4267	5.0008	0.0031	0.9945	6.1501	0.0007	0.9746

intraparticle diffusion		
k_{int} (g g^{-1} min$^{-1/2}$)	C g g^{-1}	R^2
0.2207	-0.404	0.9944

Fig. S11b (a) Pseudo-first-order, (b) pseudo-second-order and (c) intraparticle diffusion model plots for the iodine adsorption onto TPT-DHBD COF.

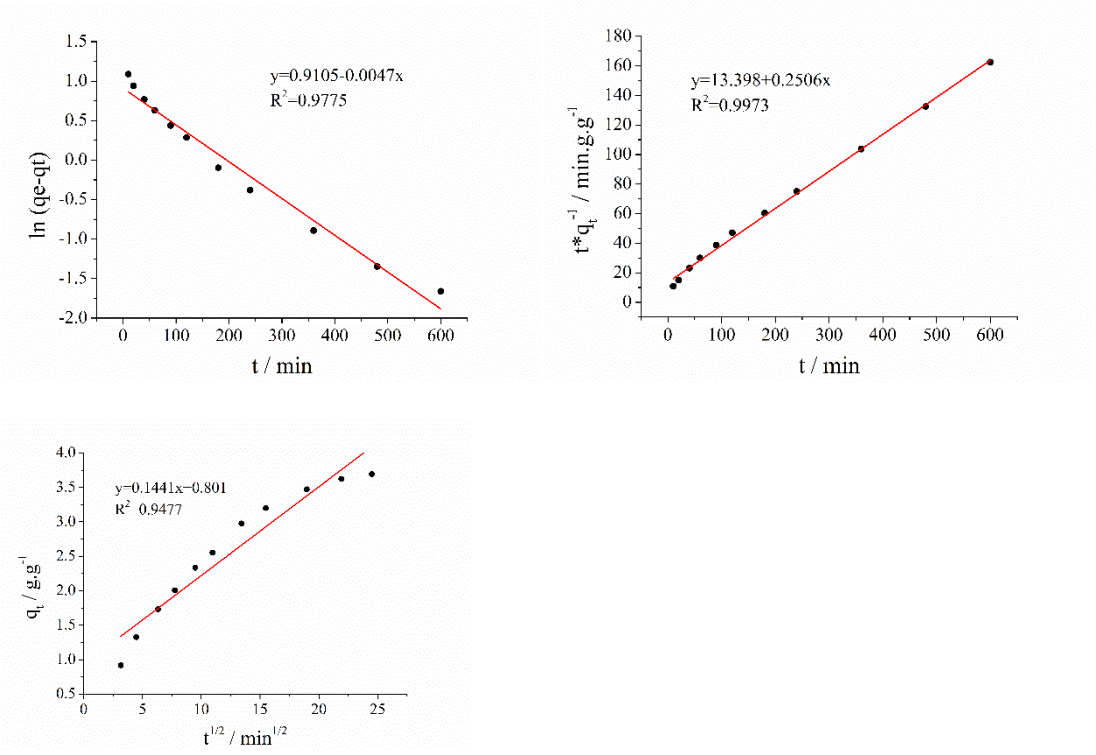

Table S4. Kinetic parameters for the iodine adsorption onto TPT-DHBD COF.

q_e (exp) (g g^{-1})	pseudo-first-order			pseudo-second-order		
	q_e (g g^{-1})	k_1 (min^{-1})	R^2	q_e (g g^{-1})	k_2 (g g^{-1} min^{-1})	R^2
3.8833	2.4856	0.0047	0.9775	3.9904	0.0047	0.9973

intraparticle diffusion		
k_{int} (g g^{-1} $min^{-1/2}$)	C g g^{-1}	R^2
0.1441	0.801	0.9477

Fig. S11c Pseudo-second order kinetic model of iodine adsorption of TPT-DHBDx COFs as a function of time at 75°C and ambient pressure.

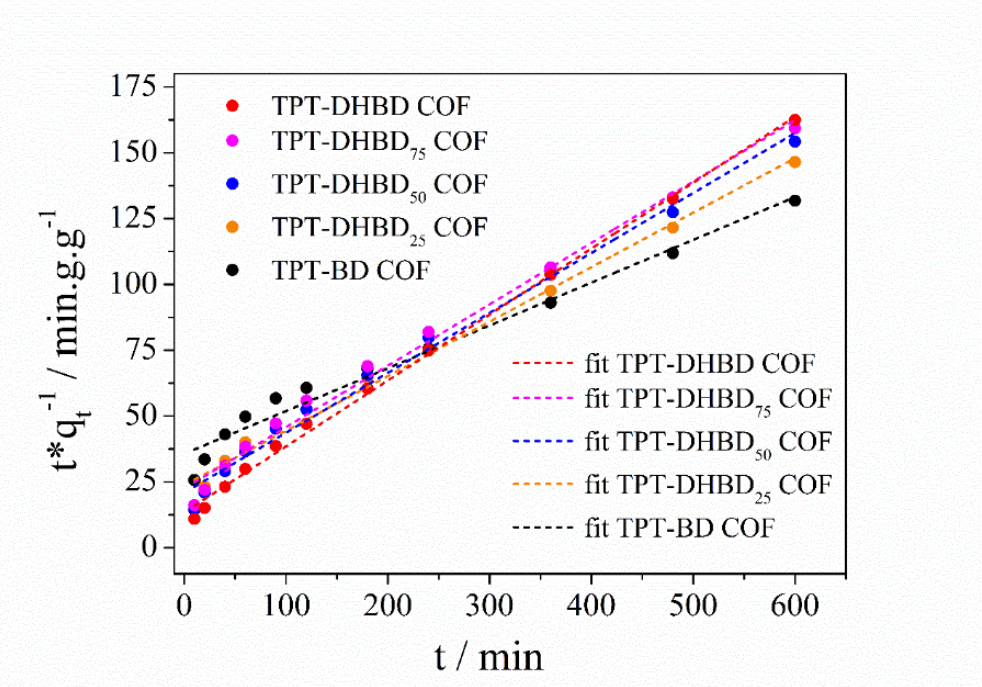

Table S5. The pseudo-second-order kinetic data of the iodine adsorption of TPT-DHBDx COFs.

Adsorbents	q_e (exp) (g g^{-1})	q_e (g g^{-1})	k_1 (min^{-1})	R^2
TPT-BD COF	5.4267	6.1501	0.0007	0.9746
TPT-DHBD$_{25}$ COF	4.6500	4.8286	0.0018	0.9888
TPT-DHBD$_{50}$ COF	4.2967	4.3917	0.0025	0.9908
TPT-DHBD$_{75}$ COF	4.1167	4.2863	0.0024	0.9912
TPT-DHBD COF	3.8833	3.9904	0.0047	0.9973

Table S6. The pseudo-first-order kinetic data of the iodine adsorption of TPT-DHBD$_X$ COFs.

Adsorbents	q_e (exp) (g g^{-1})	q_e (g g^{-1})	k_1 (min^{-1})	R^2
TPT-BD COF	5.4267	5.0008	0.0031	0.9945
TPT-DHBD$_{25}$ COF	4.6500	3.7753	0.0035	0.9826
TPT-DHBD$_{50}$ COF	4.2967	3.3311	0.0037	0.99
TPT-DHBD$_{75}$ COF	4.1167	3.2459	0.0039	0.992
TPT-DHBD COF	3.8833	2.4856	0.0047	0.9775

Theoretical and experimental values are very close to each other in Table S5, indicating the iodine adsorption of TPT-DHBD$_X$ COFs are more suitable for a pseudo-second-order kinetic model.

15. Figure S12. Gravimetric changes of iodine uptake and release of TPT-DHBD COF on a gram scale as a function of time at ambient pressure.

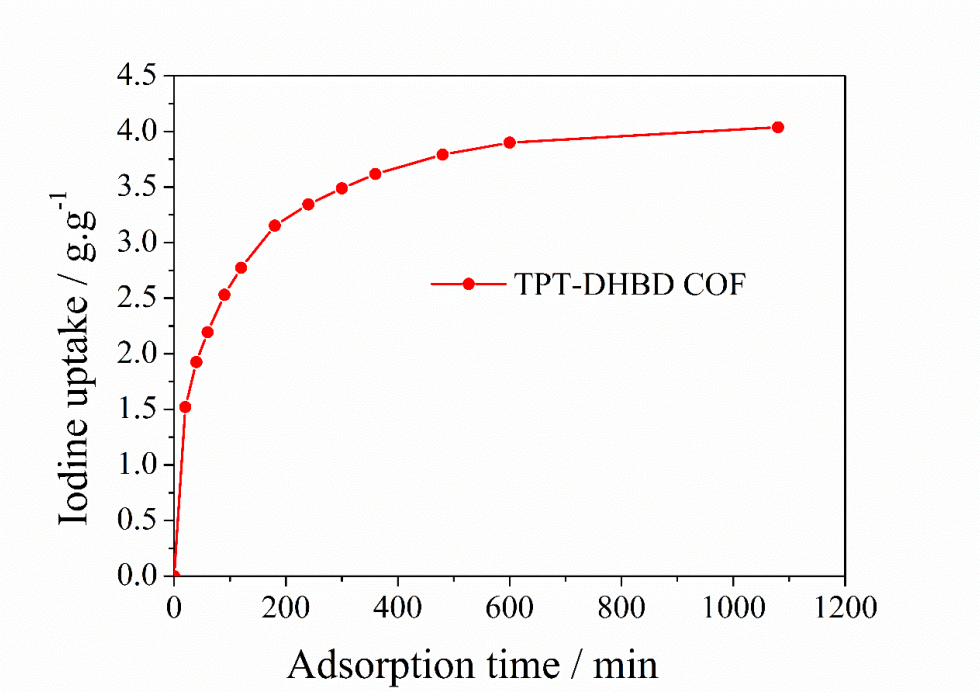

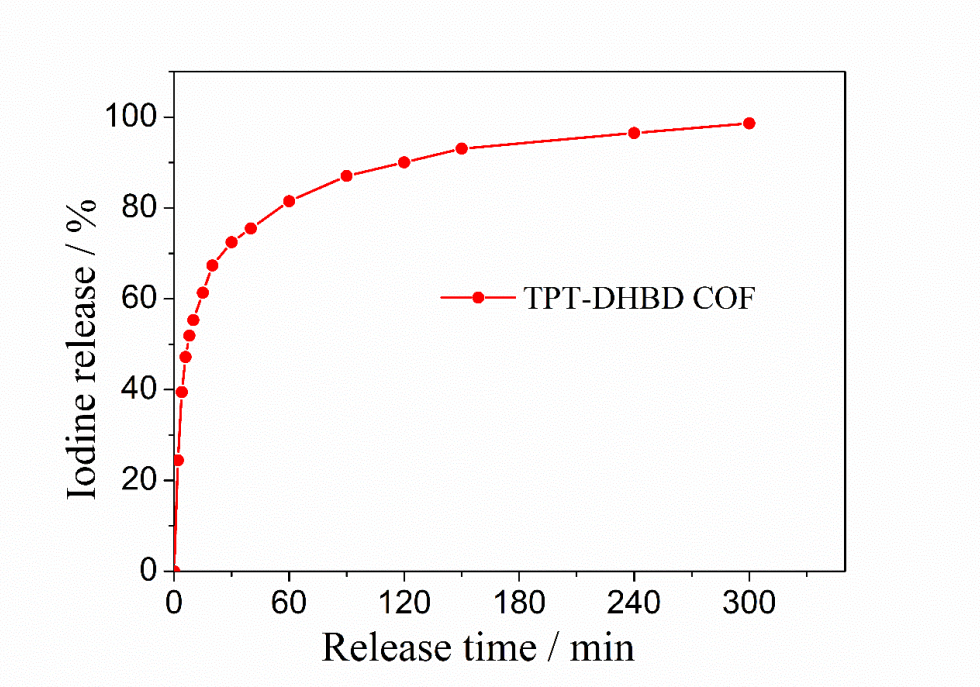

16. Figure S13. Reusability of TPT-BD COF and TPT-DHBD COF for iodine uptake.

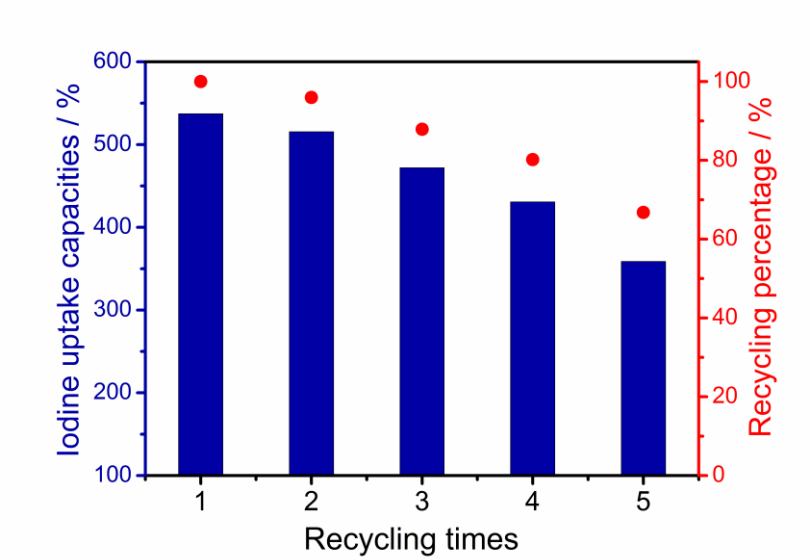

Fig. S13a Reusability of **TPT-BD COF** for iodine capture. The sample with initial iodine uptake of 537.3 wt% was used for the recycle test. (recycling parameters: 75 ℃, 48 h and 125 ℃, 360 min).

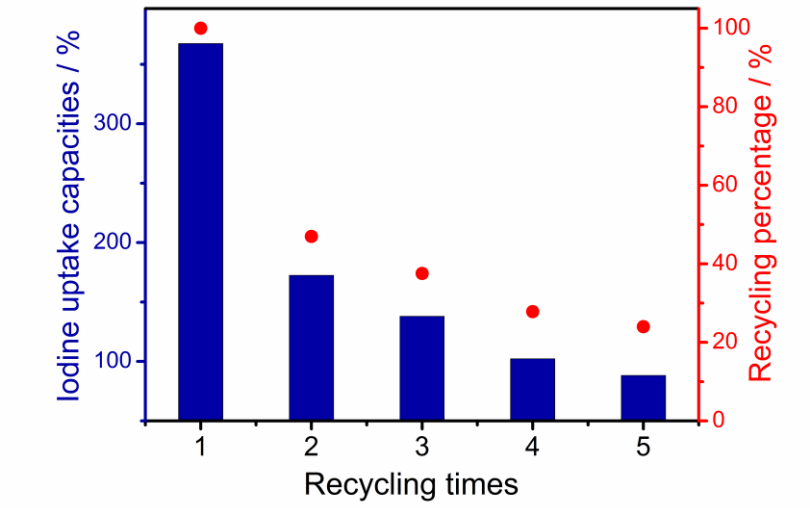

Fig. S13b Reusability of **TPT-DHBD COF** for iodine capture. The sample with initial iodine uptake of 367.5 wt % was used for the recycle test. (recycling parameters: 75 ℃, 48 h and 125 ℃, 120 min).

17. Figure S14. Photographs show the progress of the iodine enrichment in hexane.

TPT-DHBD COF

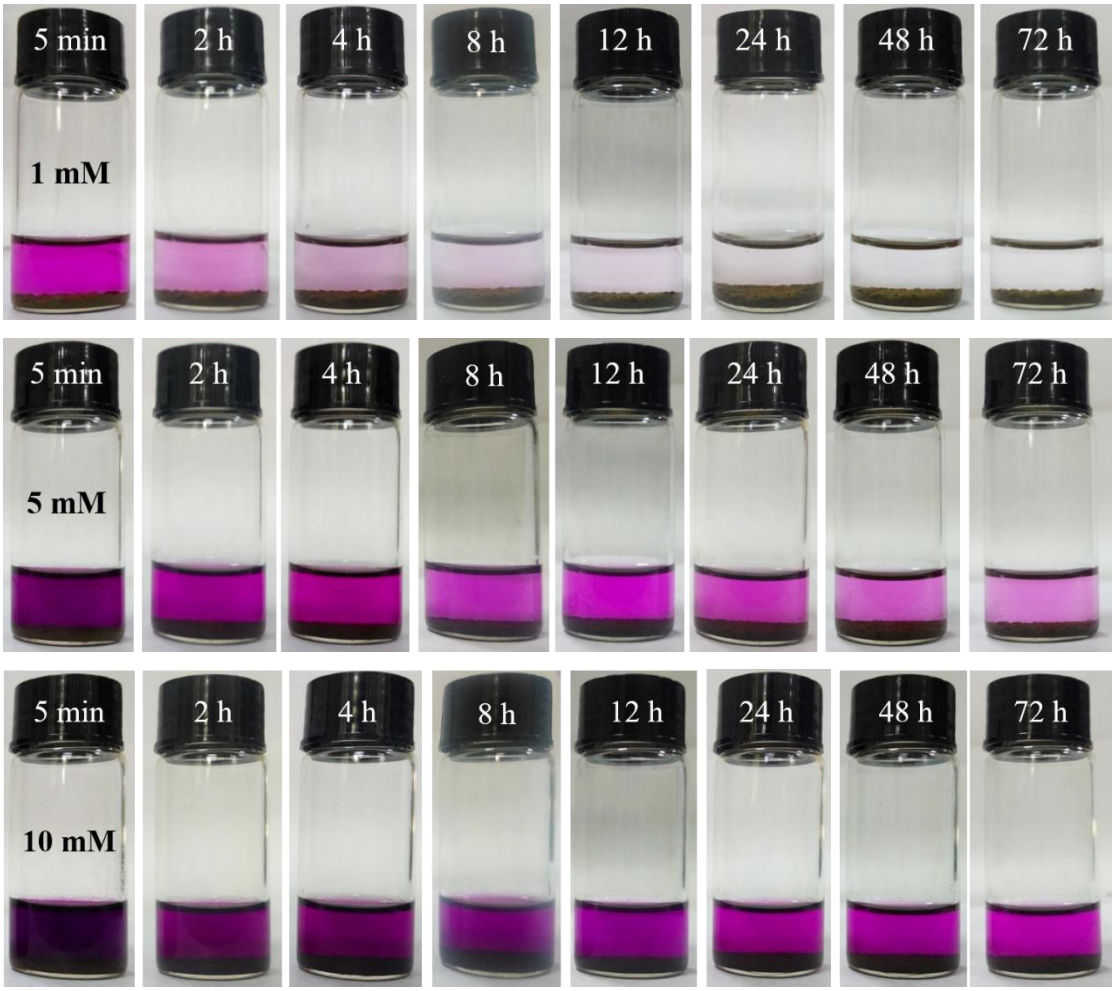

a) Photographs show the color change of iodine enrichment progress when 30 mg of TPT-DHBD COF was immersed (no stirring) in a hexane solution of iodine (1 mmol L^{-1}, 5 mmol L^{-1}, 10 mmol L^{-1}, 3 mL).

It is obvious in the photographs that TPT-DHBD COF shows faster iodine uptake efficiency in hexane solution, which means that TPT-DHBD COF also has a promising application in iodine enrichment in solution.

TPT-BD COF

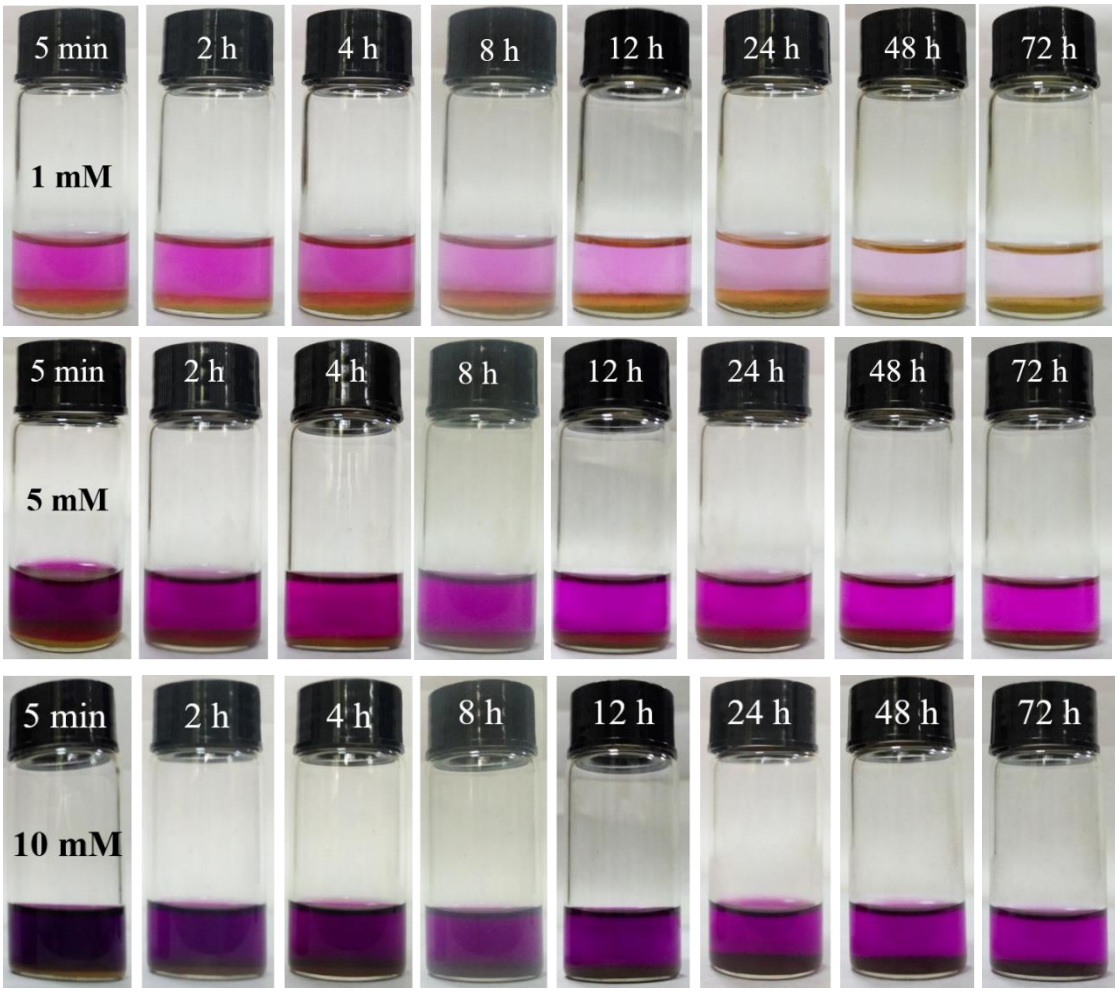

b) Photographs show the color change of iodine enrichment progress when 30 mg of TPT-BD COF was immersed (no stirring) in a hexane solution of iodine (1 mmol L^{-1}, 5 mmol L^{-1}, 10 mmol L^{-1}, 3 mL).

18. Figure S15. Photographs to show the progress of the iodine release in ethanol.

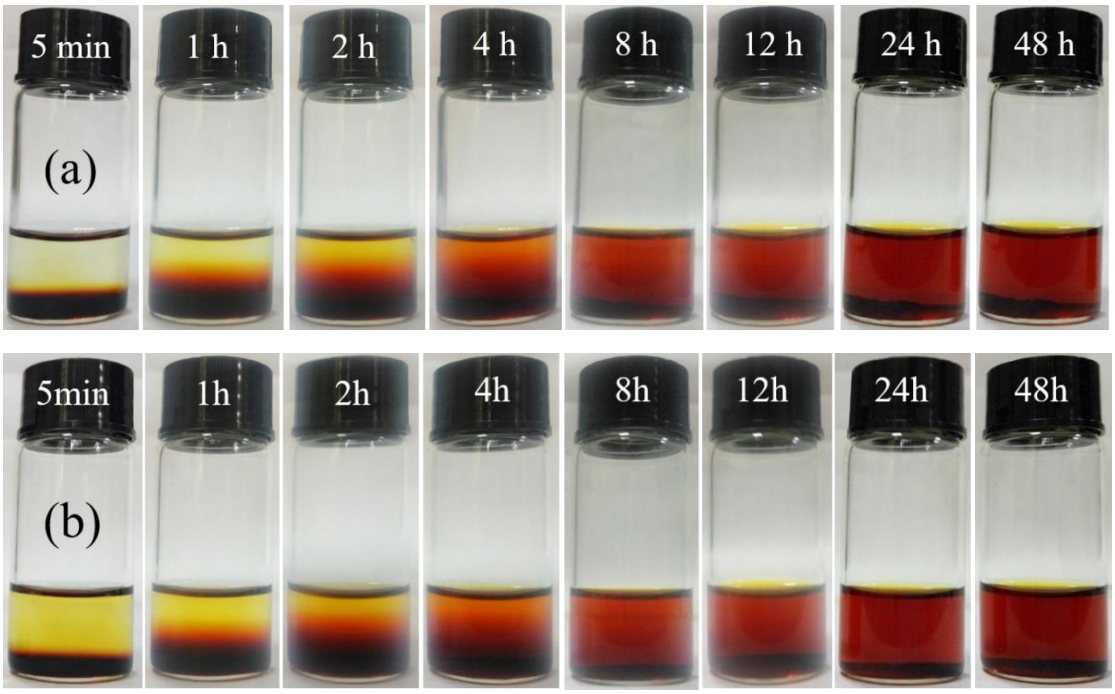

Figure S15. Photographs show the progress of the iodine release from TPT-DHBD COF@I_2 (a) and TPT-BD COF@I_2 (b), when the iodine-containing COFs are immersed in ethanol (10 mg; 4ml).

19. Table S7. Elemental analysis.

Adsorbents	Carbon	Nitrogen	Oxygen	Hydrogen	Yield %
TPT-BD COF	72.80	11.36	11.49	4.35	61.3
TPT-DHBD$_{25}$ COF	71.19	11.21	13.15	4.46	59.8
TPT-DHBD$_{50}$ COF	69.34	10.87	15.52	4.27	78.4
TPT-DHBD$_{75}$ COF	67.29	10.87	17.63	4.21	68.7
TPT-DHBD COF	65.46	9.87	20.63	4.05	62.4

20. Table S8. Iodine uptake data with time.

Table S8 Gravimetric iodine uptake data for TPT-DHBD$_X$ COFs as a function of time at 75 ℃.

Adsorbents	**6h**		**12h**		**32h**		**46h**
	Ads$_{I2}$ g/g	**Percent %**	**Ads$_{I2}$ g/g**	**Percent %**	**Ads$_{I2}$ g/g**	**Percent %**	**Ads$_{I2}$ g/g**
TPT-BD COF	3.87	71.27	4.70	86.56	5.29	97.42	5.43
TPT-DHBD$_{25}$ COF	3.69	79.35	4.23	90.97	4.57	98.28	4.65
TPT-DHBD$_{50}$ COF	3.42	79.53	3.96	92.09	4.22	98.14	4.30
TPT-DHBD$_{75}$ COF	3.38	82.04	3.84	93.20	4.05	98.30	4.12
TPT-DHBD COF	3.47	89.43	3.69	95.10	3.84	98.97	3.88

21. Table S9. Iodine release data with time.

Table S9 Gravimetric iodine release data for TPT-DHBD$_X$ COFs as a function of time at 125 ℃.

Adsorbents	5min	10min	40min	90min	180 min	360 min	420 min
	Iodine release / %						
TPT-BD COF	47.74	61.64	80.36	87.09	91.69	94.29	94.75
TPT-DHBD$_{25}$ COF	42.34	57.78	79.58	87.66	93.55	98.18	98.15
TPT-DHBD$_{50}$ COF	41.10	56.84	81.08	88.79	94.70	98.29	98.29
TPT-DHBD$_{75}$ COF	39.13	55.82	82.12	89.32	96.22	98.71	99.70
TPT-DHBD COF	48.69	62.52	83.20	92.24	97.47	100.00	99.89

22. Table S10. Porosity parameters and iodine uptake.

Table S10. Porosity parameters of TPT-DHBD$_X$ COFs studied in present work and iodine uptake.

Adsorbents	S_{BET} (m^2/g)	V_{total} (cm^3/g)	D_{pore} (nm)	Iodine capacity (mg I_2/g)
TPT-BD COF	109	0.30	3.43	5430
TPT-DHBD$_{25}$ COF	188	0.32	3.43	4650
TPT-DHBD$_{50}$ COF	124	0.19	3.43	4300
TPT-DHBD$_{75}$ COF	157	0.19	3.43	4120
TPT-DHBD COF	297	0.54	3.18	3880

23. Table S11. Comparison of iodine uptake properties of porous materials.

Adsorbents	Temperature (℃)	pressure	S_{BET} (m^2/g)	Iodine capacity (mg I_2/g)	References
TPT-BD COF	75	1 bar	109	5430	This work
TPT-DHBD$_{25}$ COF	75	1 bar	188	4650	This work
TPT-DHBD$_{50}$ COF	75	1 bar	124	4300	This work
TPT-DHBD$_{75}$ COF	75	1 bar	157	4120	This work
TPT-DHBD COF	75	1 bar	297	4030	This work
SIOC-COF-7	75	1 bar	618	4810	11
TTPB	75	1 bar	222	4430	12
HCMP-2, -3	85	1 bar	153, 82	3160, 3360	13
BDP-CPP-1, -2	75	1 bar	635, 235	2830, 2230	14
CMPN-2, -3	70	1 bar	339, 1368	1100, 2080	15
Azo-Trip	77	1 bar	510	2330	16
NiP-CMP	77	1 bar	2630	2020	17
ZIF-8	77	1 bar	1630	1250	18
Cu-BTC	75	1 bar	---	1750	19
Ag@Mon-POF	70	1 bar	690	250	20
Ag@Zeolite Mordenites	95	1 bar	---	275	21
Activated carbon	75	1 bar	---	300	22

References

1. You, G.; Cheng, Z.; Peng, H.; He, H. The synthesis and characterization of a novel phosphorus–nitrogen containing flame retardant and its application in epoxy resins. *J. Appl. Polym. Sci.* **2014**, *131*.41079.

2. Hohenberg, P.; Kohn, W. Inhomogeneous electron gas. *Phys. Rev.* **1964**, *136*, B864-B871.

3. Kohn, W.; Sham, L. Self-consistent equations including exchange and correlation effects. J. *Phys. Rev.* **1965**, *140*, A1133- A1138.

4. Frisch, M. J.; Trucks, G. W.; Schlegel, H. B.; Scuseria, G. E.; Robb, M. A.; Cheeseman, J. R.; Scalmani, G.; Barone, V.; Mennucci, B.; Petersson, G. A.; Nakatsuji, H.; Caricato, M.; Li, X.; H. P. H.; Izmaylov, A. F.; Bloino, J.; Zheng, G.; Sonnenberg, J. L.; Hada, M.; Ehara, M.; Toyota, K.; Fukuda, R.; Hasegawa, J.; Ishida, M.; Nakajima, T.; Honda, Y.; Kitao, O.; Nakai, H.; Vreven, T.; Jr., J. A. M.; Peralta, J. E.; Ogliaro, F.; Bearpark, M.; Heyd, J. J.; Brothers, E.; Kudin, K. N.; Staroverov, V. N.; Kobayashi, R.; Normand, J.; Raghavachari, K.; Rendell, A.; Burant, J. C.; Iyengar, S. S.; Tomasi, J.; Cossi, M.; Rega, N.; Millam, J. M.; Klene, M.; Knox, J. E.; Cross, J. B.; Bakken, V.; Adamo, C.; Jaramillo, J.; Gomperts, R.; Stratmann, R. E.; Yazyev, O.; Austin, A. J.; Cammi, R.; Pomelli, C.; Ochterski, J. W.; Martin, R. L.; Morokuma, K.; Zakrzewski, V. G.; Voth, G. A.; Salvador, P.; Dannenberg, J. J.; Dapprich, S.; Daniels, A. D.; Farkas, Ö.; Foresman, J. B.; Ortiz, J. V.; Cioslowski, J.; Fox, D. J. Gaussian 09, Revision D.01. Gaussian, Inc.: Wallingford, CT, 2009.

5. Becke, A. D. Density-functional thermochemistry. III. The role of exact exchange. *J. Chem. Phys.* **1993**, *98*, 5648-5652.

6. Lee, C.; Yang, W.; Parr, R. G. Development of the Colle-Salvetti correlation-energy formula into a functional of the electron density. *Phys. Rev. B: Condens. Matter Mater. Phys.* **1988**, *37*, 785-789.

7. Mayer, I. On bond orders and valences in the ab initio quantum chemical theory. *Int. J. Quantum Chem.* **1986**, *29*, 73-84.

8. Mayer, I. Bond orders and valences from ab initio wave functions. *Int. J. Quantum Chem.* **1986**, *29*, 477-483.

9. Angyan, J. G.; Loos, M.; Mayer, I. Covalent bond orders and atomic valence indices in the topological theory of atoms in molecules. *J. Phys. Chem.* **1994**, *98*, 5244-5248.

10. Kaur, G.; Singh, S.; Sreekumar, A.; Choudhury, A. R. The evaluation of the role of C–H⋯ F hydrogen bonds in crystal altering the packing modes in the presence of strong hydrogen bond. Journal of Molecular Structure. *J. Mol. Struct*. **2016**, *1106*, 154-169.

11. Yin, Z. J.; Xu, S. Q.; Zhan, T. G.; Qi, Q. Y.; Wu, Z. Q.; Zhao, X. Ultrahigh volatile iodine uptake by hollow microspheres formed from a heteropore covalent organic framework. *Chem. Commun.* **2017**, *53*, 7266-7269.

12. Geng, T.; Zhu, Z.; Zhang, W.; Wang, Y. A nitrogen-rich fluorescent conjugated microporous polymer with triazine and triphenylamine units for high iodine capture and nitro aromatic compound detection. *J. Mater. Chem. A* **2017**, *5*, 7612-7617.

13. Liao, Y.; Weber, J.; Mills, B. M.; Ren, Z.; Faul, C. F. Highly efficient and reversible iodine capture in hexaphenylbenzene-based conjugated microporous polymers. *Macromolecules* **2016**, *49*, 6322-6333.

14. Zhu, Y.; Ji, Y.-J.; Wang, D.-G.; Zhang, Y.; Tang, H.; Jia, X.-R.; Song, M.; Yu, G.; Kuang, G.-C. BODIPY-based conjugated porous polymers for highly efficient volatile iodine capture. *J. Mater. Chem. A* **2017**, ***5***, 6622-6629.

15. Chen, Y.; Sun, H.; Yang, R.; Wang, T.; Pei, C.; Xiang, Z.; Zhu, Z.; Liang, W.; Li, A.; Deng, W. Synthesis of conjugated microporous polymer nanotubes with large surface areas as absorbents for iodine and CO 2 uptake. *J. Mater. Chem. A* **2015**, *3*, 87-91.

16. Dang, Q. Q.; Wang, X. M.; Zhan, Y. F.; Zhang, X. M. An azo-linked porous triptycene network as an absorbent for CO 2 and iodine uptake. *Polym. Chem.* **2016**, **7**, 643-647.

17. Sigen, A.; Zhang, Y.; Li, Z.; Xia, H.; Xue, M.; Liu, X.; Mu, Y. Highly efficient and reversible iodine capture using a metalloporphyrin-based conjugated microporous polymer. *Chem. Commun*. **2014**, *50*, 8495-8498.

18. Sava, D. F.; Rodriguez, M. A.; Chapman, K. W.; Chupas, P. J.; Greathouse, J. A.; Crozier, P. S.; Nenoff, T. M. Capture of volatile iodine, a gaseous fission product, by zeolitic imidazolate framework-8. *J. Am. Chem. Soc.* **2011**, *133*, 12398-12401.

19. Sava, D. F.; Chapman, K. W.; Rodriguez, M. A.; Greathouse, J. A.; Crozier, P. S.; Zhao, H. Y.; Chupas, P. J.; Nenoff, T. M. Competitive I2 sorption by Cu-BTC from humid gas streams. *Chem. Mater*. **2013**, *25*, 2591-2596.

20. Katsoulidis, A. P.; He, J.; Kanatzidis, M. G. Functional monolithic polymeric organic framework aerogel as reducing and hosting media for Ag nanoparticles and application in capturing of iodine vapors. *Chem. Mater.* **2012**, *24*, 1937-1943.

21. Chapman, K. W.; Chupas, P. J.; Nenoff, T. M. Radioactive iodine capture in silver-containing mordenites through nanoscale silver iodide formation. *J. Am. Chem. Soc.* **2010**, *132*, 8897-8899.

22. Ma, H.; Chen, J. J.; Tan, L.; Bu, J. H.; Zhu, Y.; Tan, B.; Zhang, C. Nitrogen-Rich Triptycene-Based Porous Polymer for Gas Storage and Iodine Enrichment. *ACS Macro. Lett.* **2016**, *5*, 1039-1043.